İSTANBUL TECHNICAL UNIVERSITY ★ INSTITUTE OF SCIENCE AND TECHNOLOGY

VOLTAGE REGULATION OF A VARIABLE-SPEED PERMANENT-MAGNET SYNCHRONOUS ALTERNATOR FOR VEHICULAR ELECTRIC SYSTEMS

M.S. Thesis by

Berker BİLGİN

Department : Interdisciplinary

Programme: Mechatronics Engineering

JUNE 2008

İSTANBUL TECHNICAL UNIVERSITY ★ INSTITUTE OF SCIENCE AND TECHNOLOGY

VOLTAGE REGULATION OF A VARIABLE-SPEED PERMANENT-MAGNET SYNCHRONOUS ALTERNATOR FOR VEHICULAR ELECTRIC SYSTEMS

M.S. Thesis by
Berker BİLGİN
(518041005)

Date of submission : 2 May 2008

Date of defence examination: 10 June 2008

Supervisor (Chairman): Asst. Prof. Dr. Levent OVACIK

Members of the Examining Committee Asst. Prof. Dr. Deniz YILDIRIM

Asst. Prof. Dr. Metin AYDIN (K.Ü.)

JUNE 2008

İSTANBUL TEKNİK ÜNİVERSİTESİ ★ FEN BİLİMLERİ ENSTİTÜSÜ

ARAÇ ELEKTRİK SİSTEMLERİ İÇİN DEĞİŞKEN HIZLI SABİT MIKNATISLI SENKRON GENERATÖRÜN GERİLİM REGÜLASYONU

YÜKSEK LİSANS TEZİ

Berker BİLGİN
(518041005)

Tezin Enstitüye Verildiği Tarih : 2 Mayıs 2008
Tezin Savunulduğu Tarih : 10 Haziran 2008

Tez Danışmanı : Yrd. Doç. Dr. Levent OVACIK
Diğer Jüri Üyeleri Yrd. Doç. Dr. Deniz YILDIRIM
Yrd. Doç. Dr. Metin AYDIN (K.Ü.)

HAZİRAN 2008

PREFACE

During my professional carrier in the automotive industry as an electrical engineer, I have been both in development stage and the field. I have experienced that, especially in luxury cars, vehicle electrical systems are approaching their limits. Besides, the cost of the hardware and software to control the system within these limits are increasing rapidly.

It is obvious that the future of the automotive industry is hybrid and electrical vehicles. However it is not obvious when this time will come and the new technology will spread out to the market. I believe that this substantial change will take time and during this time the automotive industry is going to keep developing and producing fossil fuel powered vehicles, legislations are going to keep restricting the industry to develop more environmental friendly vehicles and customers are going to keep demanding more technological vehicles. Therefore, for the near future, vehicle electrical system should be revised and redesigned to increase the efficiency and power density as it has been done in this thesis.

I would like to say thanks to my supervisor Assistant Prof. Dr. Levent OVACIK, who has always been a guide for me to achieve this thesis and my friends and my family, who always supported me during my entire graduate studies.

May 2008 Berker BİLGİN

CONTENTS

Abbreviations

CPSR	: Constant Power Speed Range
DOC	: Depth-of-Charge
EMF	: Electromotive Force
EMSM	: Electrically Magnetized Synchronous Machine
IPM	: Interior Permanent Magnet
PMSM	: Permanent Magnet Synchronous Machine
PWM	: Pulse-Width Modulation
REDOX	: Reduction-Oxidation
SCR	: Silicon-Controlled Rectifier
SMR	: Switched-Mode Rectifier
SOC	: State-of-Charge
VOC	: Open Circuit Voltage

LIST OF TABLES

LIST OF FIGURES

LIST OF SYMBOLS

B-	: Battery negative terminal
B+	: Battery positive terminal
C	: SMR capacitance
$\mathbf{C_1}$	: Over voltage capacitance
$\mathbf{C_b}$	: Capacitor representing battery capacity
D-	: Alternator negative terminal
d	: Duty-cycle
D+	: Alternator positive terminal
DF	: Alternator field winding
$\mathbf{E_{cd}}$	: Energy drawn in discharging or transferred in charging
$\mathbf{E_d}$	: Induced voltage on d-axis
$\mathbf{E_f}$	: Induced voltage
$\mathbf{E_L}$	: Energy left
$\mathbf{E_{max}}$	: Maximum available energy
$\mathbf{E_{max,\ cor}}$	: Temperature corrected maximum energy
$\mathbf{E_q}$	: Induced voltage on d-axis
$\mathbf{G_{Bch}}$	: Transfer function of battery charging
$\mathbf{G_C}$	: Transfer function of SMR capacitance
$\mathbf{G_R}$	: Transfer function of load resistances
$\mathbf{G_{SMR}}$	: Transfer function of SMR
$\mathbf{I_a}$	: Armature current
$\mathbf{I_B}$	: Battery current
$\mathbf{I_C}$	: Current charging up SMR capacitor
$\mathbf{I_d}$	: d-axis current
$\mathbf{i_f}$	: Excitation current
$\mathbf{I_G}$	: Alternator current
$\mathbf{I_{IN}}$	: Input current of SMR
$\mathbf{I_{OUT}}$	: Output current of SMR
$\mathbf{I_P}$	: Parasitic branch current
$\mathbf{I_q}$	: q-axis current
$\mathbf{I_R}$	: Vehicle electrical load current
$\mathbf{I_{sc}}$	: Short circuit current
$\mathbf{J_a}$	: Alternator inertia
$\mathbf{J_{en}}$	: Engine inertia
$\mathbf{J_{eq}}$	: Equivalent inertia
K	: Peukert constant
$\mathbf{K_{Bch}}$	: Gain of battery charging transfer function
$\mathbf{k_e}$	: Mechanical machine constant
$\mathbf{K_I}$	: Integral constant of PI controller
$\mathbf{K_P}$	: Proportional constant of PI controller
$\mathbf{L_d}$	: d-axis inductance
$\mathbf{L_q}$	: q-axis inductance

$\mathbf{n}$: Peukert exponent
$\mathbf{n_a}$: Alternator speed
$\mathbf{n_e}$: Engine speed
$\mathbf{n_i}$: Engine idle speed
$\mathbf{p}$: Number of pole pairs
$\mathbf{P_{Bch}}$: Pole of battery charging transfer function
$\mathbf{Q}$: Battery capacity
$\mathbf{R_1}$: Over voltage resistance
$\mathbf{R_{1c}}$: Charge over-voltage resistance
$\mathbf{R_{1d}}$: Discharge over-voltage resistance
$\mathbf{r_a}$: Alternator pulley diameter
$\mathbf{R_a}$: Armature resistance
$\mathbf{R_a}$: Stator phase resistance
$\mathbf{R_c}$: Total resistance for charging
$\mathbf{R_d}$: Total resistance for discharging
$\mathbf{r_{en}}$: Crankshaft pulley diameter
$\mathbf{R_L}$: Load resistances
$\mathbf{R_P}$: Self-discharge resistance
$\mathbf{R_s}$: Internal resistance
$\mathbf{R_{sc}}$: Internal resistance for charge
$\mathbf{R_{sd}}$: Internal resistance for discharge
$\mathbf{T}$: Temperature
T15 : Switch-controlled plus from ignition switch
T30 : Line from battery positive terminal (direct)
T31 : Return line from battery negative terminal or ground (direct)
$\mathbf{T_a}$: Alternator input torque
$\mathbf{T_{en}}$: Engine output torque
$\mathbf{V_B}$: Battery voltage
$\mathbf{V_{DC}}$: Output voltage of vehicle electrical system
$\mathbf{V_s}$: Source voltage
$\mathbf{V_t}$: Output voltage of alternator (rms)
$\mathbf{V_X}$: Voltage over SMR switch
$\mathbf{X_d}$: d-axis reactance
$\mathbf{X_q}$: q-axis reactance
$\mathbf{X_s}$: Synchronous reactance
$\mathbf{Z_{Bch}}$: Zero of battery charging transfer function
$\mathbf{\Theta_a}$: Alternator pulley position
$\mathbf{\Theta_{en}}$: Crankshaft pulley position
$\mathbf{\omega_a}$: Alternator pulley angular frequency
$\mathbf{\omega_e}$: Electrical angular frequency
$\mathbf{\omega_{en}}$: Crankshaft pulley angular frequency
$\mathbf{\omega_m}$: Mechanical angular frequency

ARAÇ ELEKTRİK SİSTEMLERİ İÇİN DEĞİŞKEN HIZLI SABİT MIKTANISLI SENKRON GENERATÖRÜN GERİLİM REGÜLASYONU

ÖZET

Günümüzde güç aktarımından konfor öğelerine, aktif ve pasif güvenlik sistemlerinden iletişim ve eğlence arabirimlerine kadar mekatronik ve elektrik sistemleri otomobil endüstrisinin her yerindedir. Ayrıca, kullanıcıların araçtan beklentileri yükselmekte, yasalar sıkılaşmakta ve yoğun trafik nedeniyle motorların düşük devirlerde çalışma süreleri uzamaktadır. Bu nedenle yıllardan beri büyük değişiklik göstermeyen araç elektrik sistemleri artık sınırlarına ulaşmıştır. Neredeyse tüm araç tiplerinde kullanılan Lundell-tipi alternatör teknolojisinin verimi ve bu teknolojiye uygun gerilim regülasyon sisteminin performansı yeni nesil talepleri karşılayamayacak durumdadır. Sonuç itibariyle daha verimli ve enerji yogunlugu daha yüksek bir alternatör, buna ek olarak düşük devirlerde de güç üretebilecek bir regülasyon sistemine ihtiyaç vardır. Bu çalışma kapsamında öncelikle geleneksel araç elektrik sisteminin özellikleri incelenmiştir. Kurşun-asit akünün elektriksel ve elektrokimyasal özellikleri açıklanmış ve sisteme etkisini analiz etmek amacıyla matematiksel modeli oluşturulmuştur. Bu model kullanılarak akünün şarj ve deşarj transfer fonksiyonları elde edilmiştir. İlerleyen kısımlarda yeni alternatör teknolojileri incelenmiş, bu teknolojilerin özellikleri Lundell-tipi alternatör ile kıyaslanmıştır. Sonuç olarak otomotiv sektörünün artan taleplerini karşılayabilecek sabit mıknatıslı senkron makina önerilmiştir. Zıt EMK'sı sistem geriliminden yüksek olan sabit mıknatıslı senkron makinalarda akım, devir değişiklerinden önemli ölçüde etkilenmez ve bu durumda alternatör sabit akım kaynağı olarak modellenebilir. Bu nedenle, gerilim regülasyonu için anahtarlamalı doğrultucu önerilmiş ve özellikleri incelenmiştir. Farklı hız, elektriksel yük ve akü şarj seviyesi durumlarında sistem gerilimi sabit olması gerektiğinden, kapalı çevrim kontrol sistemi tasarımı yapılmıştır. Bunun için özellikle sistemin açık çevrim transfer fonksiyonu akünün şarj durumuna göre hesaplanmıştır. Sonuç itibariyle bir PI kontrolör tasarlanmış ve yapılan simulasyonlar farklı devir, elektriksel yük ve akü şarj seviyelerinde tasarlanan kontrolörün sistem gerilimini başarıyla regüle ettiğini göstermiştir.

VOLTAGE REGULATION OF A VARIABLE-SPEED PERMANENT-MAGNET SYNCHRONOUS ALTERNATOR FOR VEHICULAR ELECTRIC SYSTEMS

SUMMARY

At present, from powertrain to active and passive security systems, from comfort systems to communication and entertainment interfaces, mechatronic and electrical systems are everywhere in the automotive industry. Besides, customer expectations are growing, legislations are getting stringent and because of heavy urban traffic conditions idle time fraction of vehicle's total travel is increasing. Therefore, conventional vehicle electrical system is approaching its capability limits, which hasn't been changed substantially for years. The Efficiency of Lundell-type alternator, which is used almost in all types of vehicles, and the voltage regulator performance of this technology are not able to compensate next generation demands. As a result, a new alternator, whose efficiency and energy density is greater, and also a voltage regulation system, which can produce power even at low speeds, are required. In this study, first the properties of conventional vehicle electrical system have been introduced. The electrical and electrochemical properties of lead-acid battery have been explained and in order to analyze its effect on the system, a mathematical model has been derived. By using this model, transfer functions for charge and discharge processes have been calculated. In the next stage, new alternator trends have been introduced and compared with Lundell technology. As a result, a permanent magnet synchronous machine has been proposed, which can be a long term solution to supplying the increasing electrical power demand of automotive industry. The output current of permanent magnet alternators, whose back-EMF is greater than output voltage, will not be significantly affected by speed; hence alternator can be modeled by a constant current source. Therefore, for the voltage regulation a switched-mode rectifier has been proposed and its operational properties have been discussed. Finally, a closed-loop voltage regulation system has been designed, because the system voltage should always be constant for variable speed, electrical load and battery state-of-charge conditions. The open-loop transfer function has been calculated as a function of battery state-of-charge and a PI controller has been designed. Simulations given in the last chapter shows that, the designed controller regulates the output voltage successfully at various speed, electrical load and state-of-charge conditions.

1. INTRODUCTION

In order to supply electric power in a motor vehicle, an efficient energy source and reliable electrical system is required. Generally vehicle electrical system consists of an alternator, which is the on-board electricity generating plant when the engine is running, a battery, which stores the electricity and cranks the engine to start it, a voltage regulator and a number of electrical consumers. The block diagram of a vehicle electrical system is given in Figure 1.1.

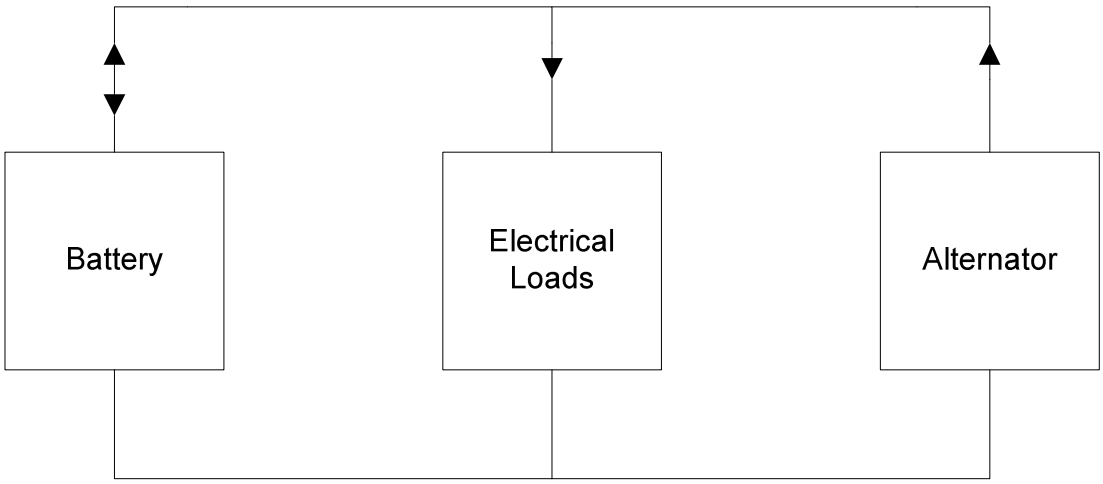

Figure 1.1: Block diagram of a vehicle electrical system

Using the electricity stored in the battery, the vehicle engine is started by the starter motor and once it's running the related control unit determines its operating conditions.

When the engine is running, the alternator supplies power which should be enough to feed the electrical consumers and charge the battery. The voltage level of the electrical system is dependent on the alternator, therefore the engine speed, and the current drawn by the electrical consumers and the battery as well.

If the consumers that are switched on create a larger current draw than the amount of power being supplied by the alternator, the electrical system voltage level drops to

the battery voltage level and the battery is discharged accordingly. In order to create a balanced electrical system, the alternator, the battery and the electrical loads should be correctly matched with each other, so that the battery is always charged sufficiently.

The electrical loads need a stable supply voltage. For example for light bulbs, voltage tolerance must be kept tight so that the bulb life and light output are within specified limits [1].

The voltage regulator prevents the voltage rising above a certain level if the possible alternator current, I_G is greater than the sum of the load current, I_R and the battery current, I_B as shown in Figure 1.2.

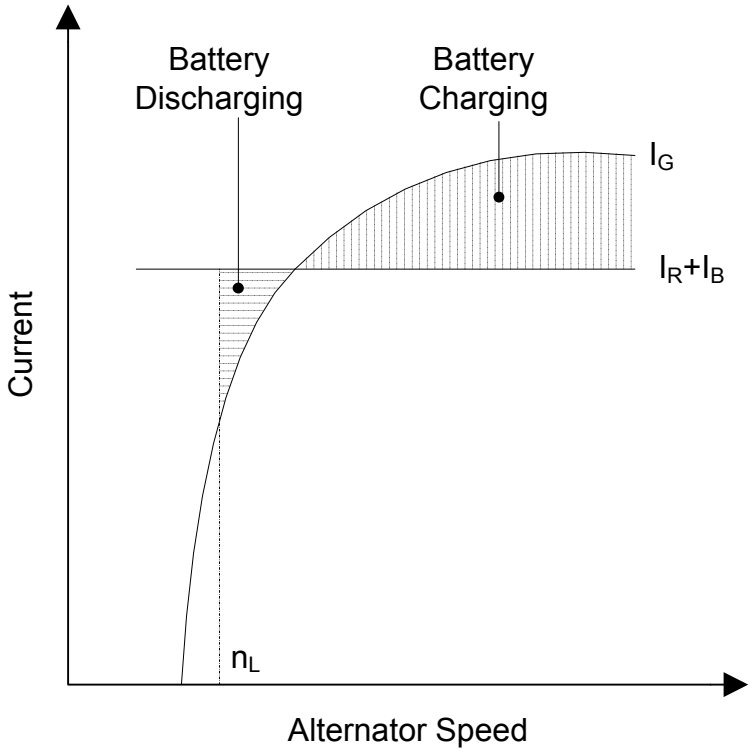

Figure 1.2: Relationship between alternator output current and load current [2]

The engine, the alternator, the battery and the electrical loads should be considered as an interrelated system. The total input-power requirements and the individual driving conditions have decisive importance with regard to the loading of the alternator and the battery [1].

As shown in Figure 1.3 the speed at which the alternator is driven, hence the alternator output current, varies with the operation of the vehicle. Performance of voltage regulator and efficiency of alternator and battery are getting more important, because over the last decade many electrical loads have been continuously added in vehicles to meet various regulations and customer demands. Also the idle time fraction of the vehicle's total travel has been increasing because of the heavy urban traffic conditions [3].

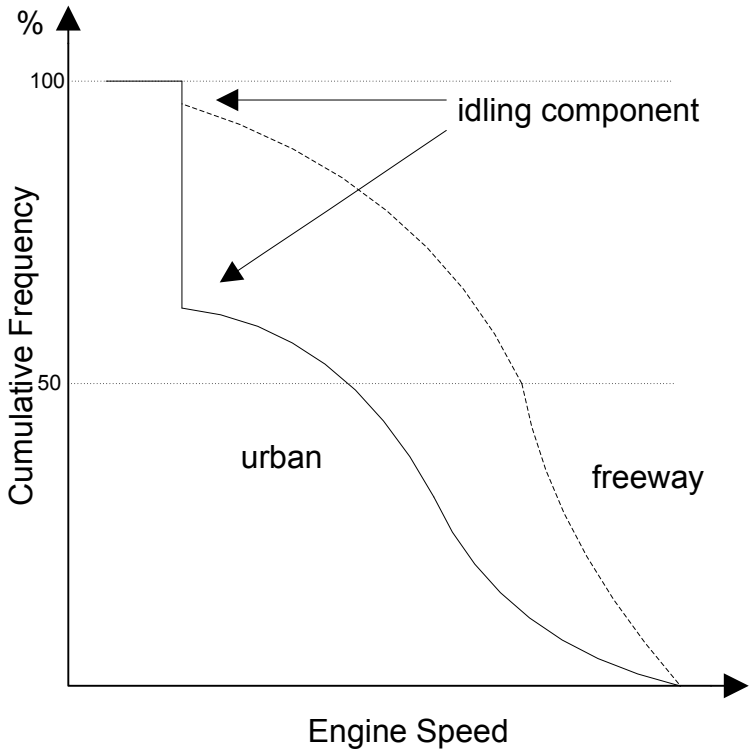

Figure 1.3: Cumulative frequency of engine speed in urban and freeway driving

1.1 Conventional Alternator

The task of the alternator is to supply energy to all current-consuming loads and is to provide the current that is sufficient to charge the battery in a normal driving cycle. The alternator is driven directly from the engine via V-belts. As the efficiency of the alternator increases with rotational speed, a high conversion ratio between the engine crankshaft and alternator is required. For passenger cars, typical value is between 1:2 and 1:3. [2]

The most common automotive generator in the market today is the Lundell-type machine [4]. Lundell-type machine is a three-phase salient pole electrically magnetized synchronous generator. A design picture of typical Lundell-type alternator is shown in Figure 1.4.

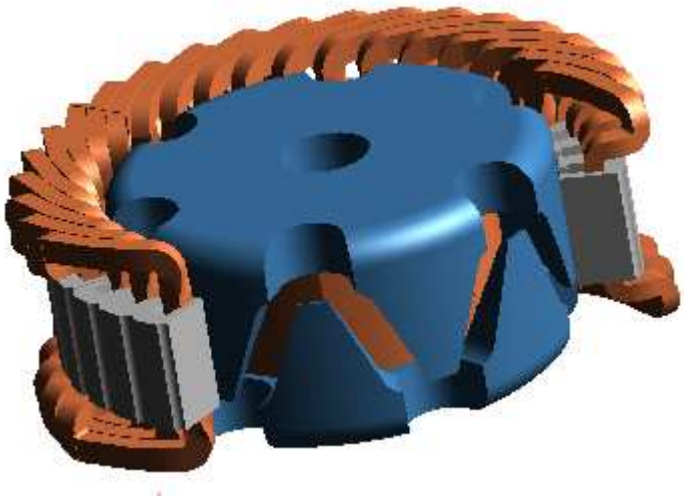

Figure 1.4: A design picture of Lundell-type machine [5]

Because of the shape of the magnetic poles of the alternator, Lundell-type machine is also designated as “claw-pole alternator”. The two oppositely-poled pole halves are attached to the rotor shaft and the claw shaped pole half fingers mesh with each other in the form of alternating north and south poles [1].

1.1.1 Output Voltage Regulation

Initially the alternator generates alternating current. But in order to power the electrical equipment of the vehicle and to charge the battery, which are designed to be operated with DC voltage, the alternating current should be rectified. Furthermore, the voltage output should be kept as constant as possible and the battery should always be charged across the complete engine speed range, independent of load conditions of the alternator.

Figure 1.5 shows the circuit diagram of a Lundell-type machine’s voltage regulator. The AC voltage produced by the alternator is rectified by a three-phase bridge rectifier. Lundell-type machine is an electrically magnetized synchronous machine,

thus the excitation current is produced by a half-wave rectifier and is connected to the armature winding.

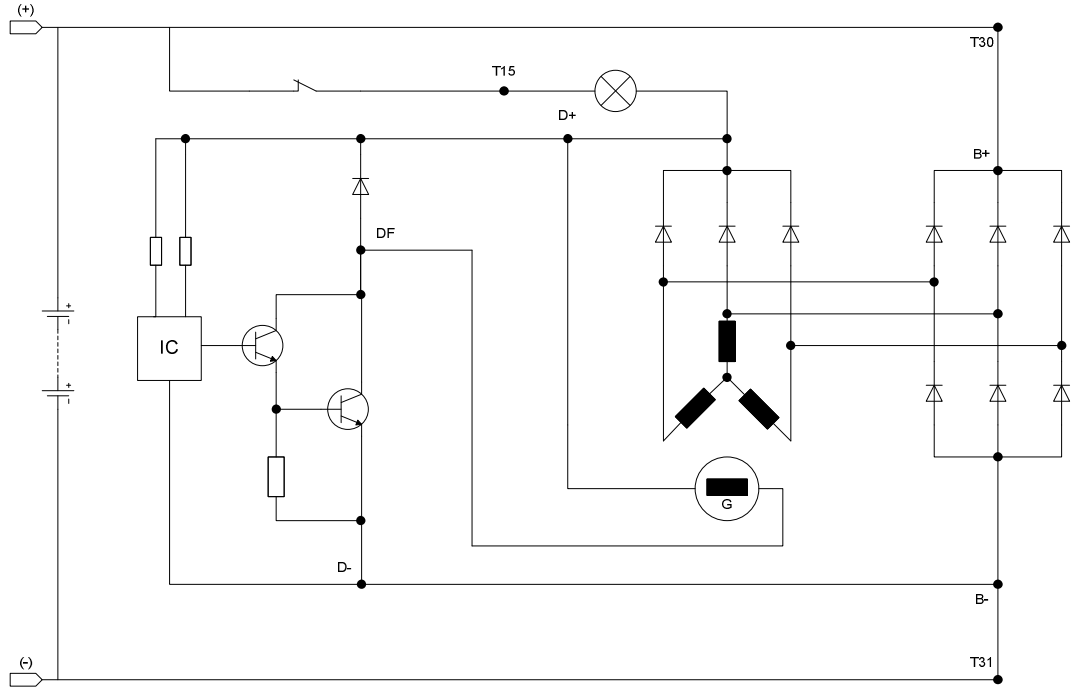

Figure 1.5: Circuit diagram of the voltage regulator of a Lundell-type machine [1]

The rectifier diodes prevent the battery to get discharged through the three-phase armature windings. Since, with the engine stopped, or when it runs too slowly for self-excitation to take place (e.g. cranking), without the diodes, current would flow through the armature windings. Nevertheless, when the alternator voltage is zero or low with respect to battery voltage, rectifier diodes are reverse biased [2].

With the engine running, the voltage level of the vehicle electrical system is dependent on the alternator itself, thus the alternator can be regarded as a standalone power generator. Presuming constant excitation current, the alternator output voltage varies with the alternator speed and load current as shown in Equation (1.1). The electrical angular frequency ω_e is proportional to the alternator mechanical speed and the number of pole pairs, *p*.

$$V_s = k_e \cdot \omega \cdot i_f - I_a \cdot R_a \qquad \textbf{(1.1)}$$

$$\omega_e = 2\pi \frac{p \cdot n_a}{60} \quad \textbf{(1.2)}$$

The voltage regulator is mounted inside the alternator together with the brushes and controls the level of excitation current, therefore the strength of rotor's magnetic field by applying a high frequency switching as a function of the output voltage. If the voltage exceeds the specified value, which is stated by international standards as 14V in a vehicle equipped with a 12V battery, the regulator interrupts the excitation current. Excitation becomes weaker and the alternator voltage drops as a result. As soon as the voltage drops below the specified value, the excitation current is applied again. The process of the voltage regulation is shown in Figure 1.6 [1]**.**

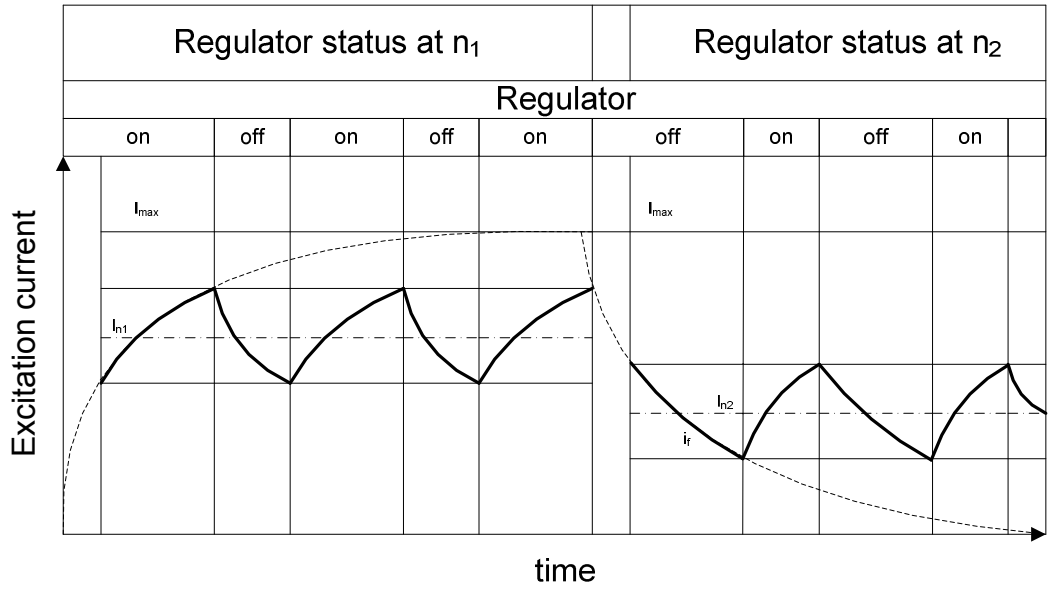

Figure 1.6: Voltage regulation in a Lundell-type machine ($n_2 > n_1$)

The characteristic curve of a vehicle alternator is shown in Figure 1.7**,** where the output voltage is already regulated to 14V by the voltage regulator. Maximum speed of the alternator is limited by the rolling bearings and the carbon brushes as well as by the cooling fan mounted to the rotor shaft.

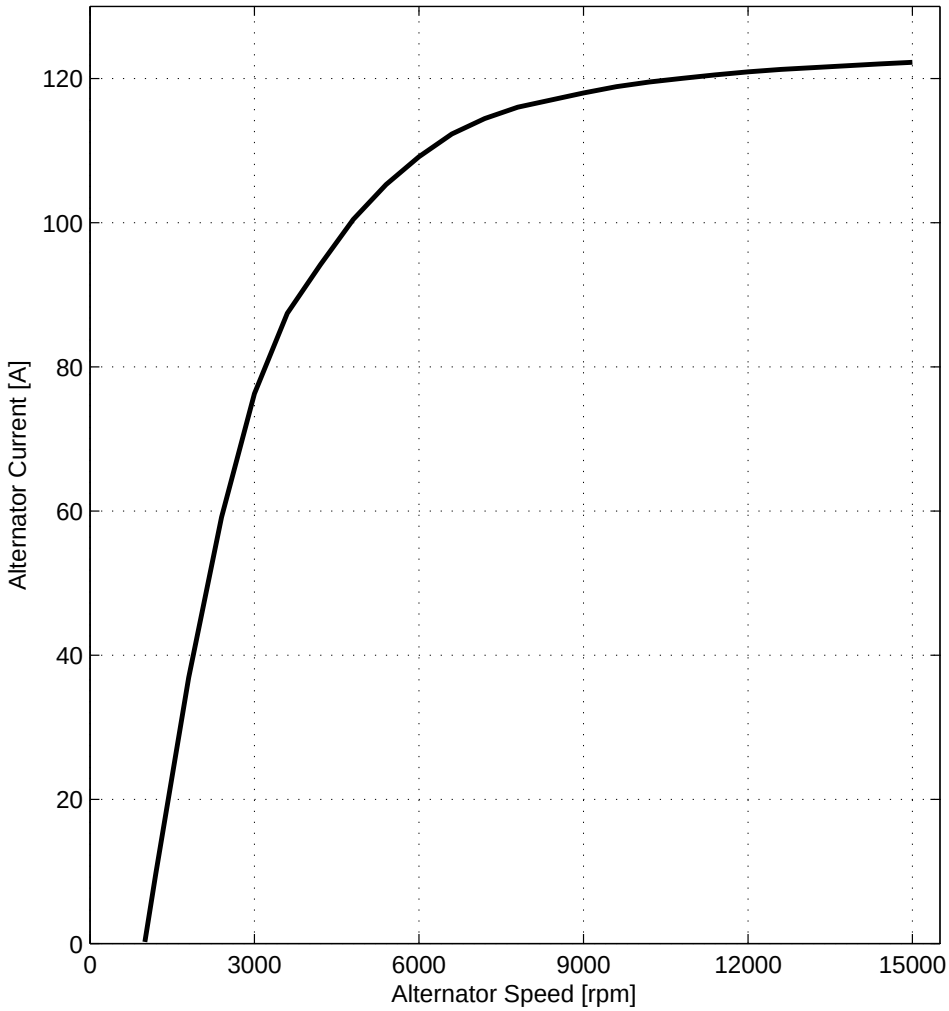

Figure 1.7: The characteristic curve of a Lundell-type machine

1.2 Lead-Acid Batteries

The battery is an integral part of vehicle electrical system. It cranks the engine by means of powering the starter, stores the electrical energy produced by the alternator with the engine running and meets the transients, while it takes a few seconds the alternator to meet the high current requirements. Lead-acid battery is a secondary battery, where charge-discharge process is essentially reversible. The characteristics of a lead-acid battery cell are given in Table 1.1.

Table 1.1: Characteristics of a Lead-Acid Battery Cell [6]

Chemistry	Anode	Pb (Metallic Lead)
	Cathode	PbO_2 (Lead Dioxide)
	Electrolyte	H_2SO_4 (Diluted sulfuric acid)
Typical Cell Voltage [V]	Nominal	2.0
	Open Circuit	2.1
	Operating	2.0-1.8
	End	1.75
Energy Density (at 20^0C)	Wh/kg	35
	Wh/L	70
Self-discharge rate (% loss/month at 20^0C)	Sb-Pb	20-30
	Maintenance Free	2-3
Life	Calendar Life (years)	2-3
	Cycle Life (cycles)	200-700
Operating Temperature [^{0}C]		-44 to 55

In automotive applications, generally lead-acid batteries are been used. This is mainly because of its high energy density, low internal resistance, wide range of operating temperature and low manufacturing costs. Besides these advantages, limited energy density, poor charge retention, lack of storability and low cycle life relatively to other secondary batteries are limitations of lead-acid batteries [6].

1.2.1 Electrochemical Process

Just like every other battery, lead-acid battery converts the chemical energy contained in its active materials directly into electrical energy by means of an electrochemical oxidation-reduction (redox) reaction. This type of reaction involves the transfer of electrons from one material to another through an electric circuit [6].

The total electrochemical reaction is shown schematically in Figure 1.8. In a discharged cell, both electrodes are lead sulfate ($PbSO_4$) and the electrolyte is dilute sulfuric acid, where 17% of the electrolyte is pure sulfuric acid (H_2SO_4) and 83% is water (H_2O). To charge the lead-acid cell the poles are connected to a DC source, whose voltage is greater than the battery voltage, thus the introduced energy forces the cell to be charged by drawing the electrons from the positive electrode and transferring to negative electrode. As a result of charging process the number of hydrogen and sulfate ions in the electrolyte are increased, thus fresh sulfuric acid (H_2SO_4) is formed and electrolyte density increases (37% sulfuric acid-63% water). When charging is completed lead sulfate ($PbSO_4$) at the positive electrode has converted to lead dioxide (PbO_2) and at the negative electrode to metallic lead (Pb).

If a lead-acid cell is overcharged electrolyte is decomposed, resulting formation of oxygen at the positive plate and hydrogen at the negative plate, which is called gassing and this reaction results with the loss of water: $H_2O \rightarrow H_2 + \frac{1}{2}O_2$ [6].

If a load is connected between the poles of a lead-acid cell, electrons flow from the negative pole to the positive pole, because of the potential difference. At the end of the discharging process lead sulfate ($PbSO_4$) is formed on both electrodes and pure sulfuric acid content of the electrolyte decreases, because oxygen atoms released from the positive electrode diffuse to the electrolyte, whereas bivalent negative sulfate ions go to both electrodes [1].

Total reaction on both electrodes is as follows. Discharge reaction takes place reversely:

Negative electrode:

$$Pb^{2+} + 2e^- \xrightarrow{charging} Pb$$

$$PbSO_4 \xrightarrow{charging} Pb^{2+} + SO_4^{2-}$$

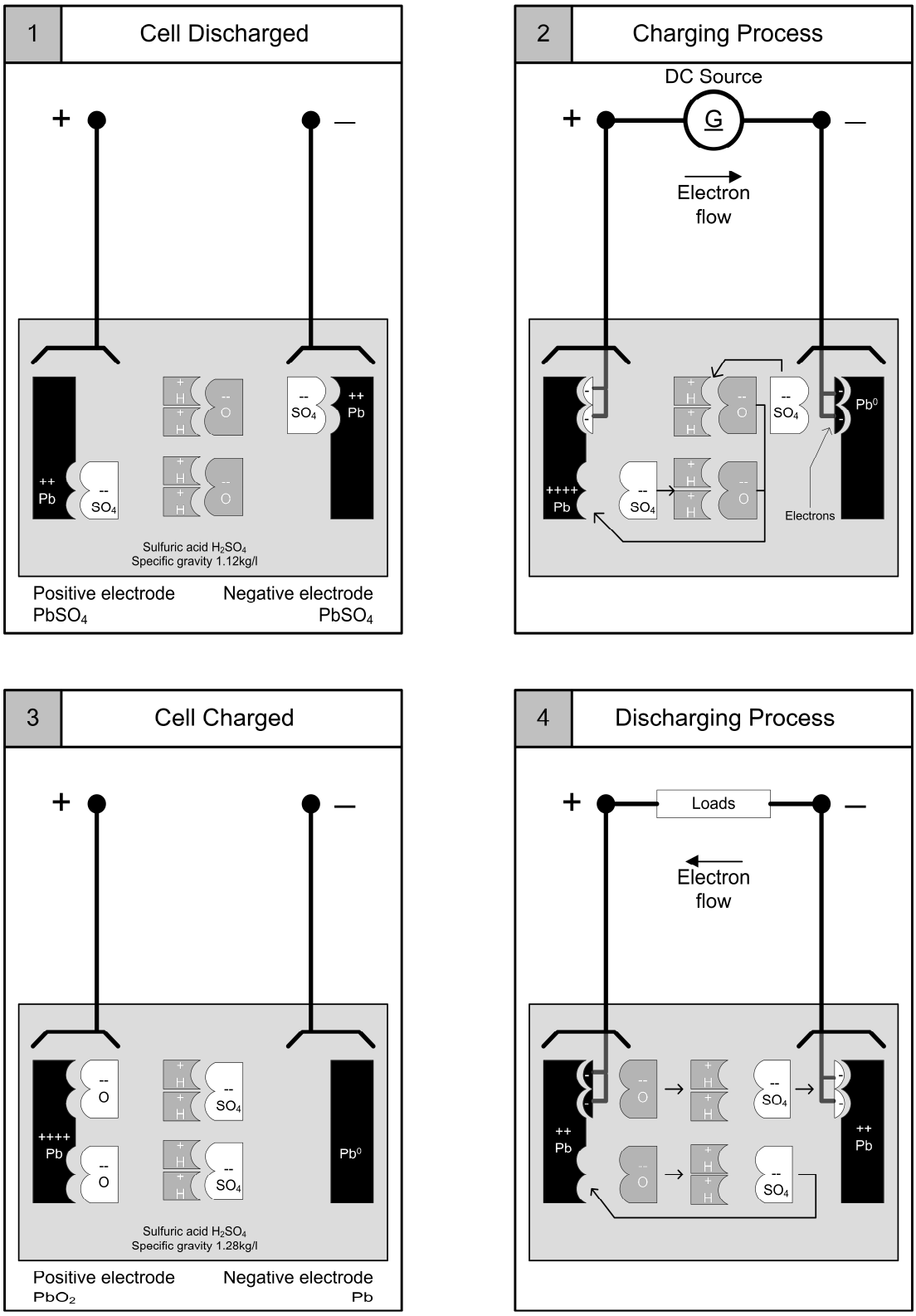

Figure 1.8: Overview of electrochemical reactions in a lead-acid battery cell [1]

1.2.2 Performance Parameters of Lead-Acid Batteries

1.2.2.1 Capacity and Discharge Current

The capacity of a battery is defined as the amount of charge that can be drawn for a length of time before the battery discharges, which is measured in units of Ampere-hours (Ah). The length of discharge does not linearly decrease with the increasing discharge current, because relationship between the available capacity and discharge current is nonlinear, due to the electrochemical properties of lead-acid battery. This nonlinear relationship is given by Peukert equation.

$$Q = K \cdot I^{1-n} \tag{1.3}$$

Where Q is the capacity in Ah, K and n are Peukert constant and exponent respectively and I is the discharge current in Amperes. Equation (1.3) shows that the higher the discharge current is, the lower are the total energy available and delivered. Figure 1.9 shows the discharge profile of an automotive battery for different discharge rates.

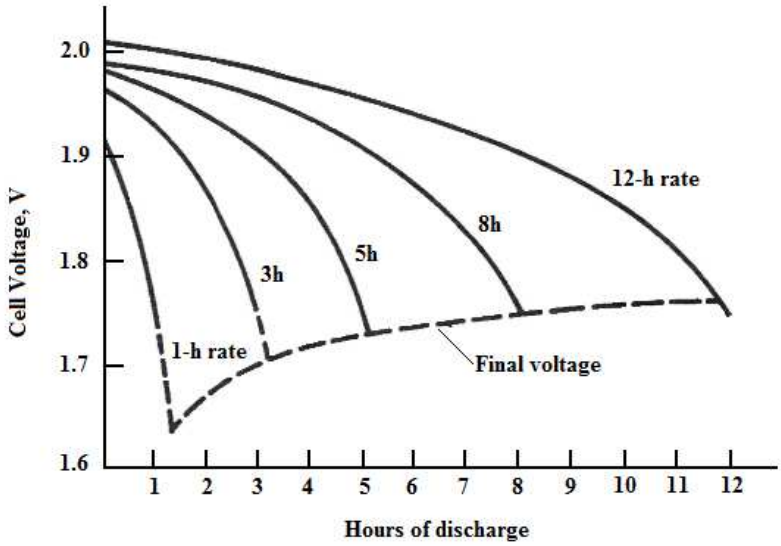

Figure 1.9: Discharge curve of a lead-acid battery for various discharge rates [6]

The Peukert effect shows itself in the electrochemical process. At higher discharge rates the electrolyte in the pore structure of the plates becomes depleted and the electrolyte cannot diffuse rapidly enough to maintain the cell voltage. Intermittent

discharge allows time for the electrolyte to recirculate, or forced circulation of the electrolyte will improve high-rate performance [6].

1.2.2.2 State-of-Charge

State-of-charge (SOC) is the amount of current that the battery can still deliver after a period of discharge or charge. As described in Section 1.2.1 the electrolyte density increases as the battery is charged, thus it is possible to understand SOC by measuring the electrolyte density.

Table 1.2: Electrolyte Density of a Lead-Acid Battery in kg/l at Different SOC [6]

State-of-Charge	Automotive Battery	Electric-Vehicle Battery	Traction Battery	Stationary Battery
100% (full charge)	1.265	1.330	1.280	1.225
75%	1.225	1.300	1.250	1.185
50%	1.190	1.270	1.220	1.150
25%	1.155	1.240	1.190	1.115
Discharged	1.120	1.210	1.160	1.080

The open circuit voltage (VOC) of a lead-acid battery is another parameter to measure SOC, because at constant temperature VOC is a function of electrolyte density as shown in Figure 1.10. Therefore, the terminal voltage of the battery is strongly dependent on SOC.

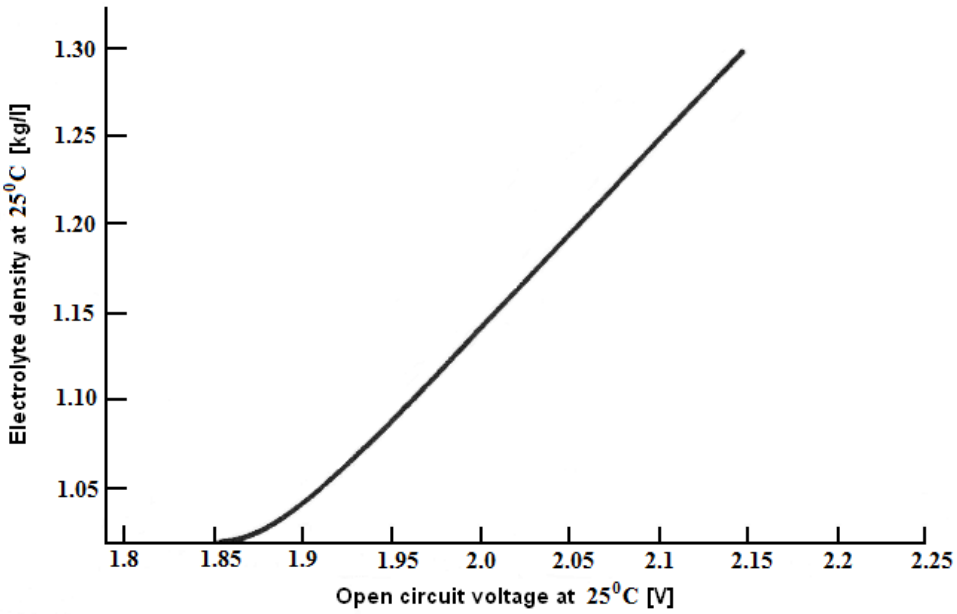

Figure 1.10: Open circuit voltage of lead-acid cell as a function of electrolyte density [6]

1.2.2.3 Effect of Temperature

The temperature at which the battery charges or discharges has a strong effect on the battery parameters. The lower the temperature is, the slower the chemical reaction takes place and the higher the internal resistance, so the power loss gets. Figure 1.11 shows the typical discharge curves for the lead-acid cell at various temperatures.

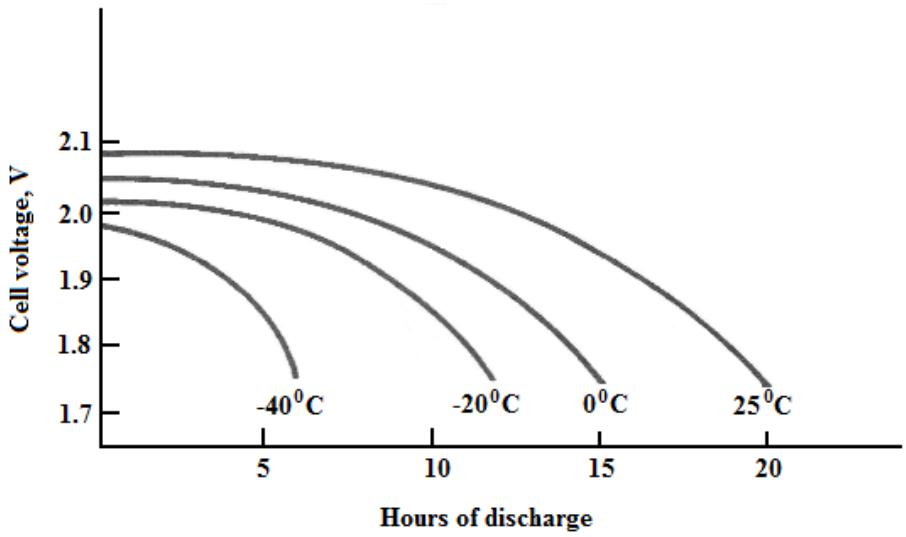

Figure 1.11: Discharge curves of a lead-acid battery at various temperatures [6]

1.2.2.4 Self Discharge

A lead-acid battery looses its capacity during open-circuit stand, which is called self-discharging. This loss is more severe with batteries which use antimonial lead grid alloys (PbSb) in the positive plate [6].

Antimony (Sb) is a hardener, which provides the lead plates the strength needed to withstand the operation in the vehicle. However, during the battery's service life the antimony is increasingly separated out due to positive-grid corrosion. This causes at first an increase at the self-discharge of negative plate and reduction at the gassing voltage; than an increase at water consumption and finally rapid discharging. In maintenance-free batteries, antimony is suppressed by calcium (Ca), which prevents negative-plate poisoning and thus self-discharging. Figure 1.12 shows the comparison of open-circuit stand loss of lead-acid batteries with different lead-grids [1].

1.2.2.5 Internal Resistance

The internal resistance of a battery is the sum of the contact resistance between the electrodes and the electrolyte (polarization resistance), resistance of electrodes

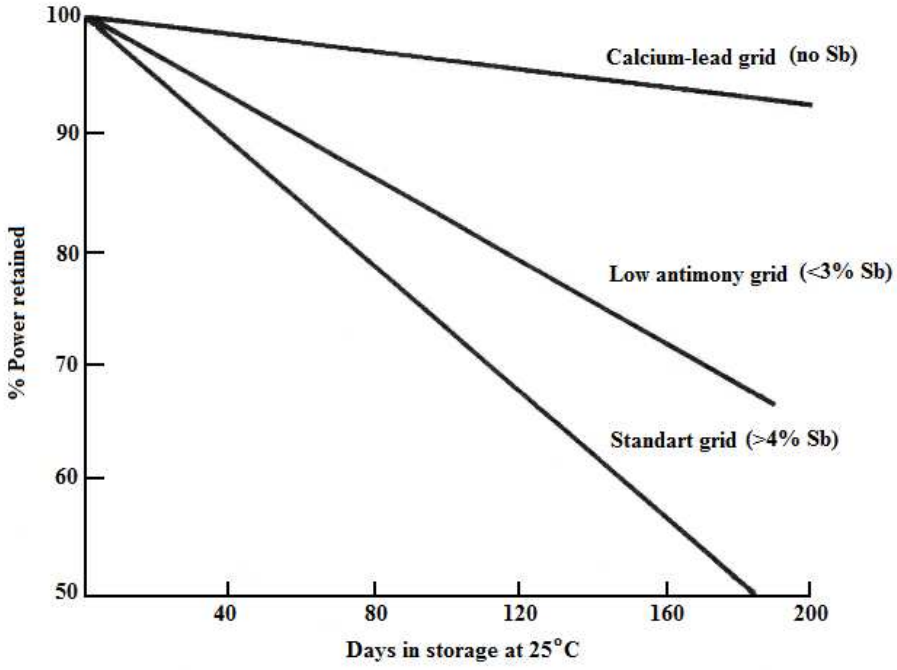

Figure 1.12: Capacity retention during stand or storage at 25^0C [6]

against the electron flow, the resistance of electrolyte against flow of ions and the resistance of cell connectors [2]. Internal resistance varies with SOC; therefore electrolyte density (Figure 1.13).

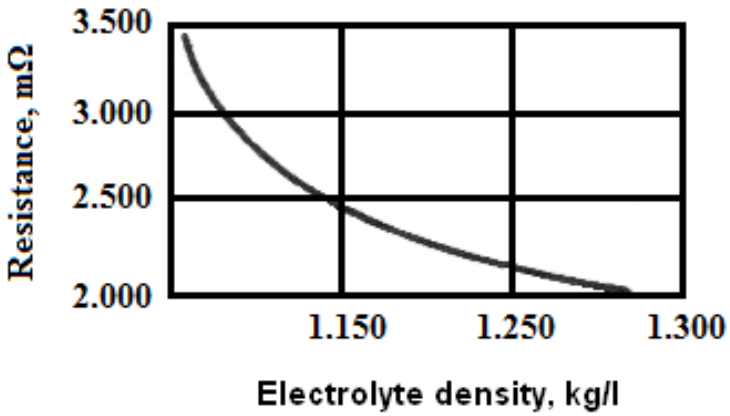

Figure 1.13: Internal resistance of a lead-acid battery during discharge [6]

2. MATHEMATICAL MODEL OF LEAD-ACID BATTERIES

The relation of the operational performance of a lead-acid battery with capacity, state-of-charge, temperature and the status of electrodes and electrolyte was stated in the previous chapter. In order to analyze the behavior of a lead-acid battery within the vehicle electrical system, it is necessary to model these electrochemical parameters by means of electrical elements (e.g. resistance, capacitance, voltage source, etc.) and to derive an equivalent circuit. In this chapter literature overview of lead-acid battery models and the model that has been used in this study is going to be introduced.

2.1 Simple Model

Figure 2.1 shows the simple model used for lead-acid batteries, which is constituted by a constant resistance and an ideal voltage source in series. The ideal voltage source expresses the open circuit voltage of the battery, whereas the resistive element the internal resistance. But as stated in Section 1.2.2 the internal resistance and VOC is highly dependent on SOC and electrolyte concentration, which makes the battery behavior nonlinear.

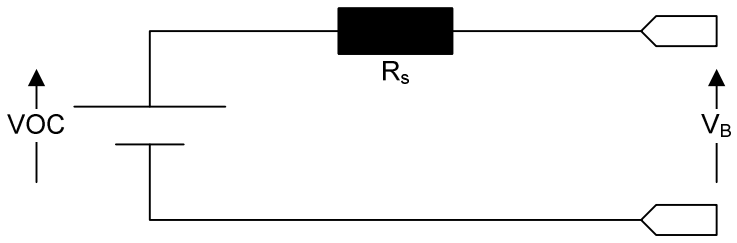

Figure 2.1: Simple model of lead-acid battery

2.2 Thevenin Model

Thevenin model of a lead-acid battery, which is shown in Figure 2.2, is another common model and is more detailed than the simple model. In this model R_s

represents the internal resistance, C_1 the over voltage capacitance and R_1 the over-voltage resistance. In Thevenin battery model the circuit elements are not functions of SOC and discharge rate.

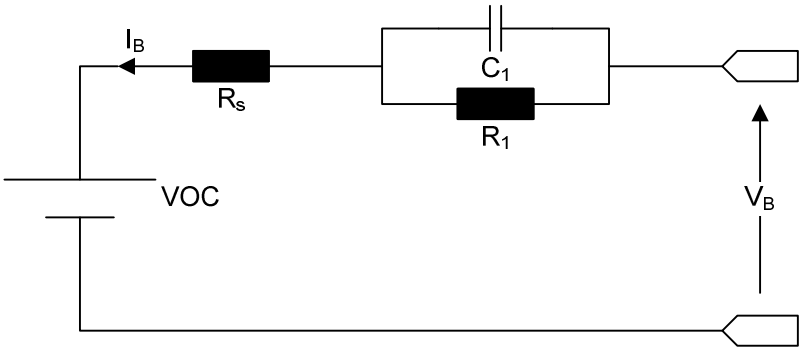

Figure 2.2: Thevenin model of lead-acid battery

2.3 Nonlinear Dynamic Model

The equivalent circuit of a nonlinear mathematical model of lead-acid battery, which has been proposed in [7], is shown in Figure 2.3. This model takes into account self-discharge, battery storage capacity, internal resistance, over voltage and environmental temperature.

C_1 is the over voltage capacitance, C_B battery capacity, I_B battery current, I_p parasitic branch current, R_{1c} charge over-voltage resistance, R_{1d} discharge over-voltage resistance, R_p self-discharge resistance, R_{sc} internal resistance for charge, R_{sd} internal resistance for discharge, V_B battery voltage, VOC open circuit voltage. The resistances are nonlinear functions of VOC and vary SOC.

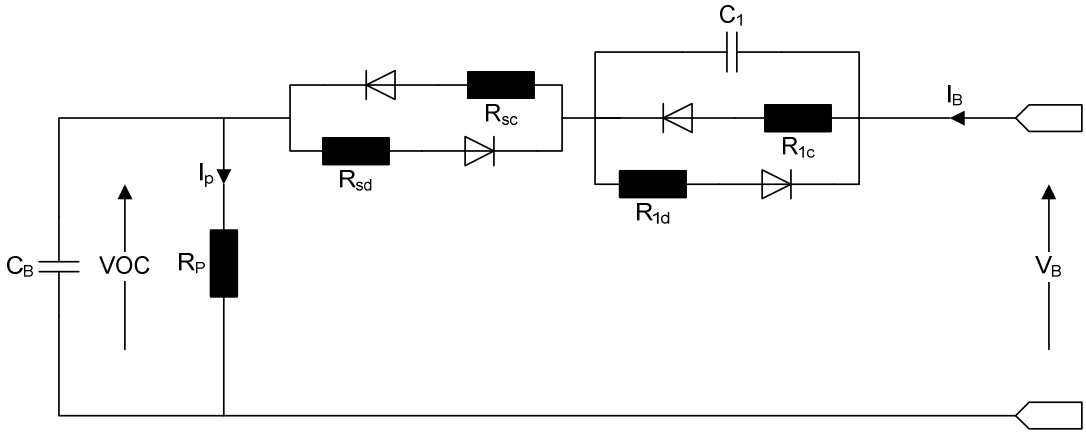

Figure 2.3: Nonlinear dynamic model of lead-acid battery

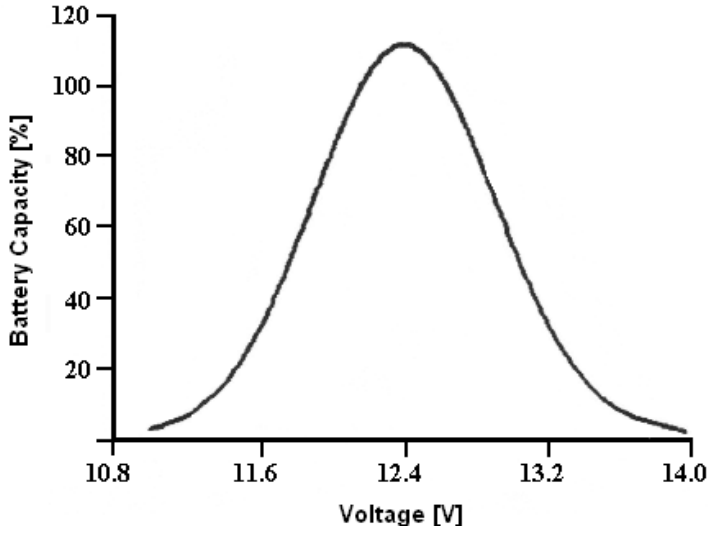

Figure 2.4: Capacity curve for nonlinear dynamic model of lead-acid battery

Although this model represents the nonlinear characteristics of the lead acid battery, the capacity, which is determined via an evaluated curve as a function of VOC (Figure 2.4), can only be modeled as a mathematical function using various mathematical parameters, resulting a complicated battery model. The curve should be chosen such that the area under the curve equals to unity.

In [8] another nonlinear dynamic model of lead-acid battery is proposed, where the parasitic branch and some elements are expressed with empirical functions. The equivalent circuit of the proposed model is shown in Figure 2.5.

In this model the energy that enters to the parasitic branch, between the nodes P and N, abandons the state of electric power and is converted into other forms of energy.

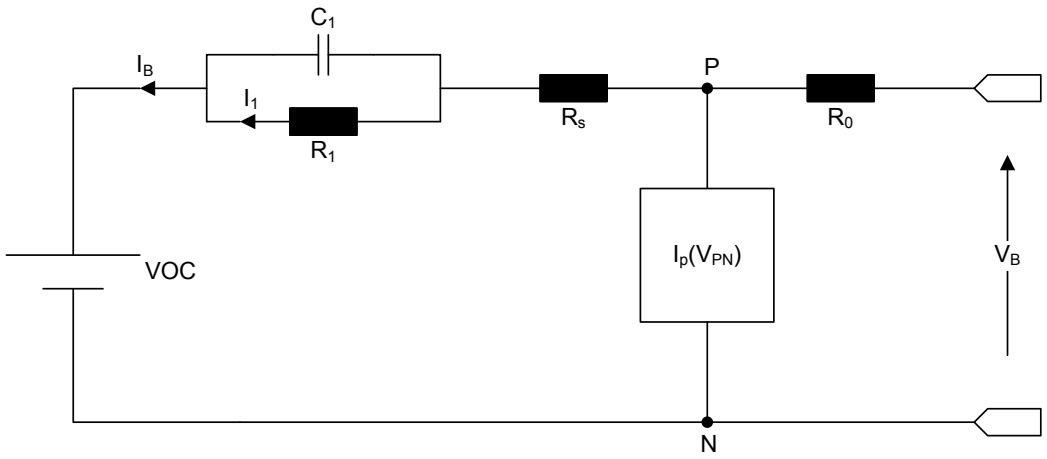

Figure 2.5: Nonlinear dynamic model of lead-acid battery with parasitic branch

For instance, the parasitic branch models the water electrolysis that occurs at the end of charging process. The main branch of the model is identified by analyzing the step response, which is measured at different values of SOC and electrolyte temperatures.

Together with SOC, in this model, a new term called depth of charge (DOC) is defined and the equations of some elements are defined by using this term. Depth of charge is the measure of discharge rate and shows how full the battery with reference to the actual discharge regime is.

This model mainly represents the characteristics of a lead-acid battery during charging process. The formula of parasitic branch current is a nonlinear function of electrolyte temperature and battery voltage. This model is not suitable to be simulated in MATLAB/Simulink by using SimPower Systems. It is better to simulate by using state-space representation, where the states are the current flowing through the resistor R_1, the battery charge level and electrolyte temperature.

2.4 Selected Model

In [9] a new dynamical model of a lead-acid battery has been proposed, where the maximum available energy, which is a nonlinear function of discharge rate and SOC, is expressed in a look up table relative to the battery open circuit voltage. This model takes into account battery storage capacity, internal resistance, self-discharge resistance, the electric losses and dependence on temperature.

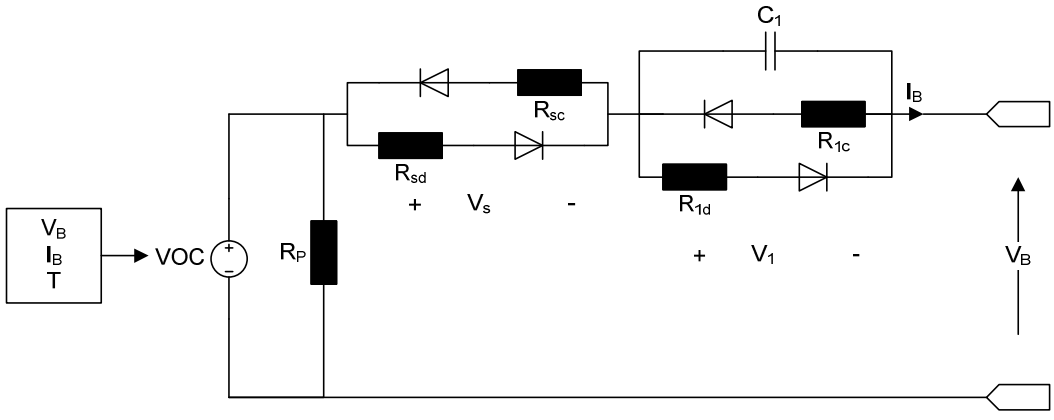

Figure 2.6: Equivalent circuit of dynamical model of lead-acid battery

The equivalent circuit of this model (Figure 2.6) is very similar to the one given in Section 2.3, distinctly VOC is represented by a voltage source, which is dependent on discharge current I_B, the energy drawn from the battery E_{cd} and the battery temperature T. The block diagram of the algorithm to determine the open circuit

voltage is given in Figure 2.7, where I_B represents the battery current, V_B the output voltage, E_{max} maximum available energy, T temperature, $E_{max,cor}$ temperature corrected maximum energy, E_{cd} energy drawn in discharging or transferred in charging, E_L energy left in the battery, VOC open circuit voltage.

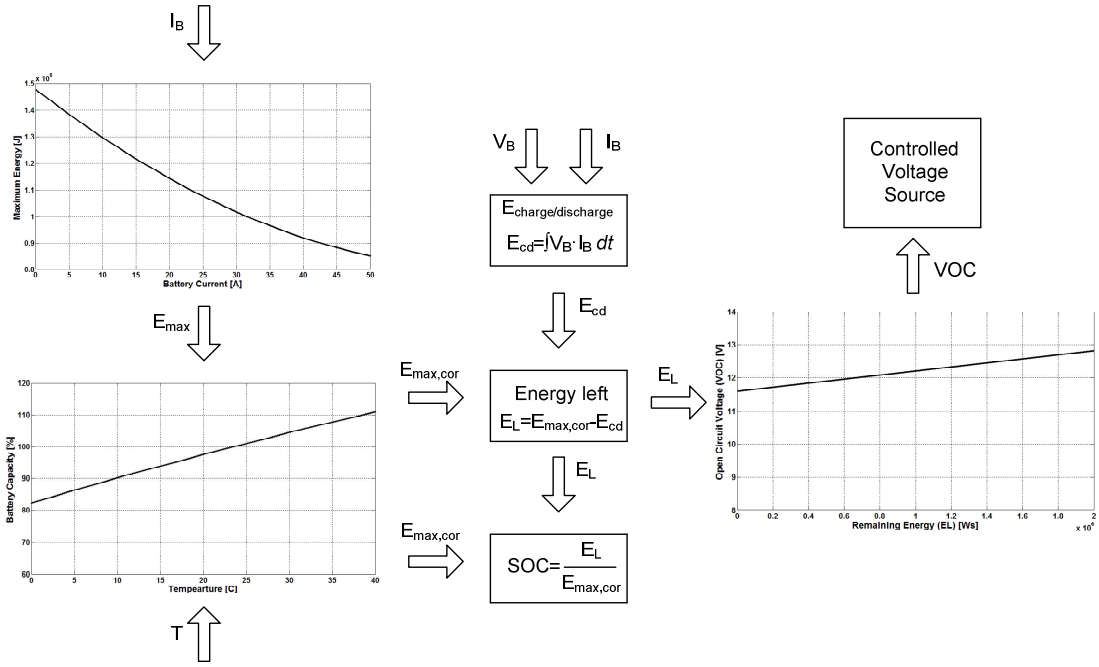

Figure 2.7: Algorithm to determine the open circuit voltage

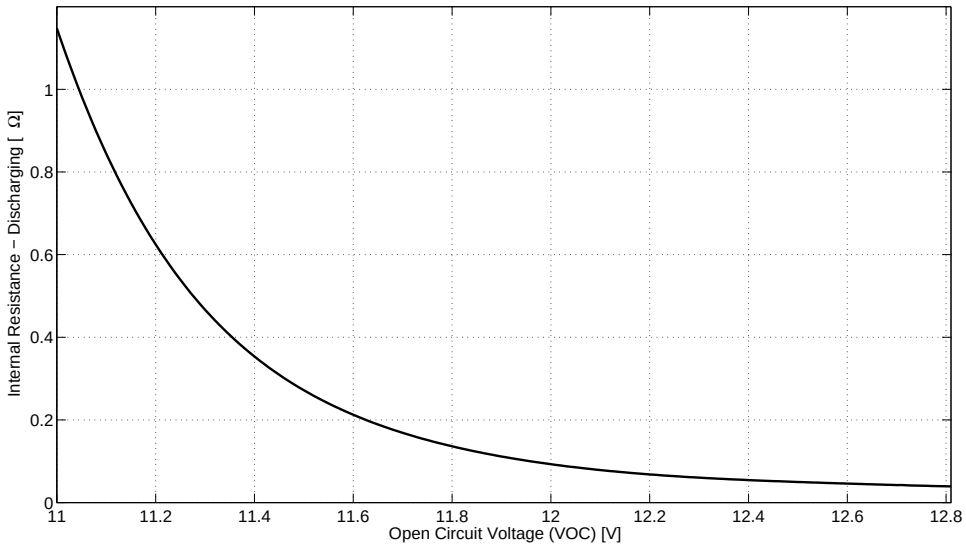

Figure 2.8: Internal resistance during discharging (R_{1d}+R_{sd})

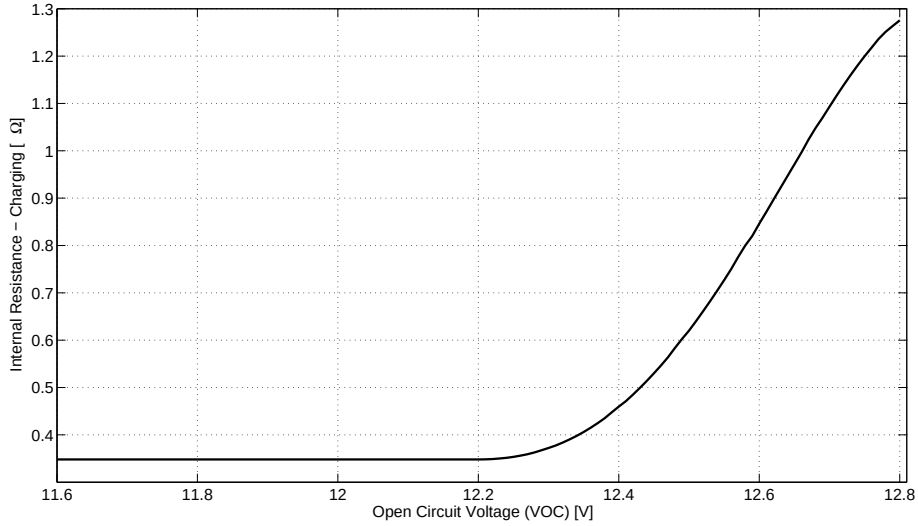

Figure 2.9: Internal resistance during charging (R_{1c}+R_{sc})

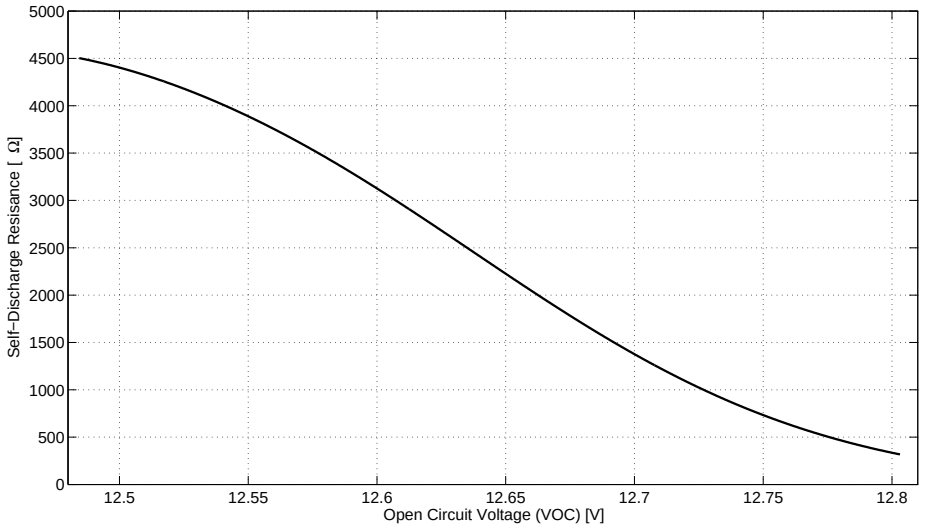

Figure 2.10: Self-discharge resistance (R_p)

As stated in Section 1.2.2.5, the internal resistance is a function of open circuit voltage, therefore battery's state-of-charge. The characteristics of the internal resistances and self-discharge resistance are given below. The internal resistance depends on the direction of current flow, which varies due to charging and discharging processes.

The model is simulated in MATLAB/Simulink. For components of equivalent circuit SimPower System blockset, for the algorithm (Figure 2.7) and circuit resistances

look-up tables are used. The simulation results of 1A, 5A and 10A discharge tests are given below.

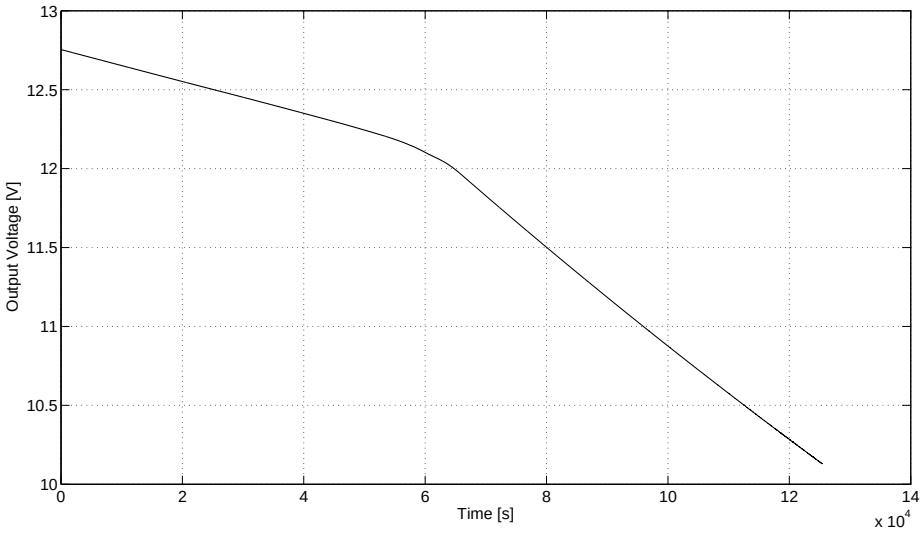

Figure 2.11: Voltage-time characteristics at 1A discharge

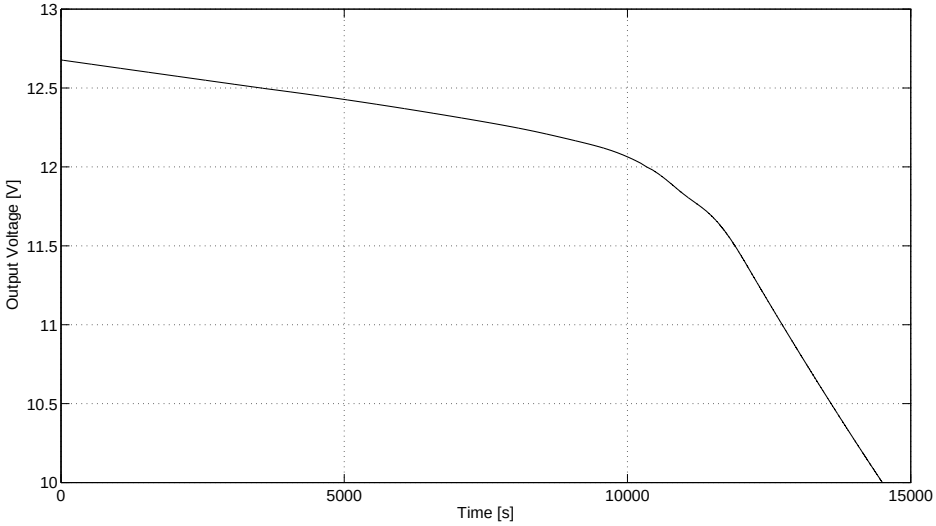

Figure 2.12: Voltage-time characteristic at 5A discharge

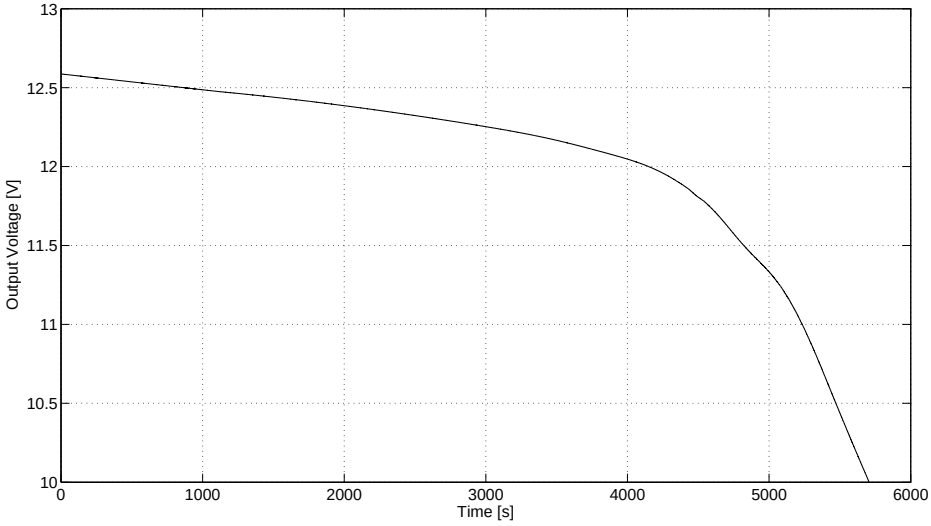

Figure 2.13: Voltage-time characteristic at 10A discharge

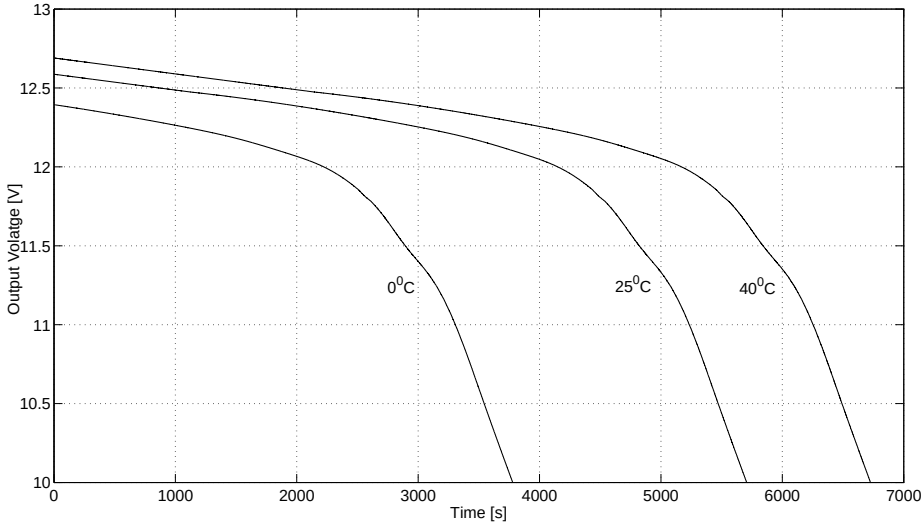

Figure 2.14: Voltage-time characteristic 10A discharge at 0^0C and 40^0C compared to standard condition discharge at 25^0C.

The effect of temperature was analyzed with a 10A constant current discharge in different temperatures. The simulation result of the temperature effect is shown in Figure 2.14.

The charging characteristic of the battery is simulated by connecting the battery to a constant 14V DC source and measuring the output voltage in a SOC range of 10% to 100%. The simulation results are shown in Figure 2.15.

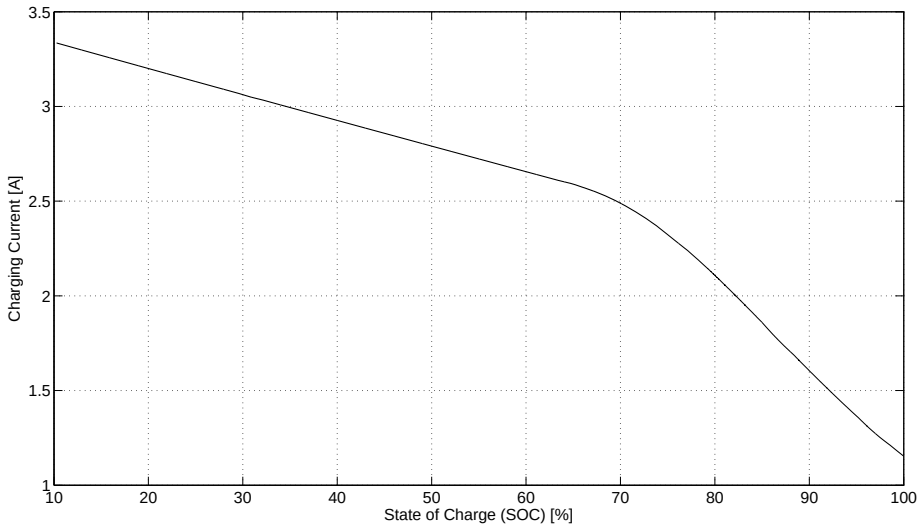

Figure 2.15: Current-SOC characteristic at 14V charging

2.4.1 Mathematical Analysis of the Lead-Acid Battery Model

The introduced lead-acid battery model is going to be used in the simulation and control system design of a vehicle electrical system, therefore the mathematical analysis and transfer function of the model should be derived. The battery's equivalent circuit, the change of its resistances along with the open circuit voltage and the algorithm to determine the open circuit voltage has been introduced previously. Note that the self-discharge resistance, R_p is connected in parallel with the open circuit voltage and as shown in Figure 2.10 its value is very high as compared with the internal resistances (Figure 2.8 and Figure 2.9). This causes a low voltage drop on the self-discharge resistance. Because of that, in the linearization process the self discharge resistance is neglected.

2.4.1.1 Charging Transfer Function

The change of the battery current under constant voltage charge was shown in Figure 2.15. The charging transfer function should express the change of the output current under a specific terminal voltage and SOC. The block diagram of equivalent circuit for charging process is shown in Figure 2.16.

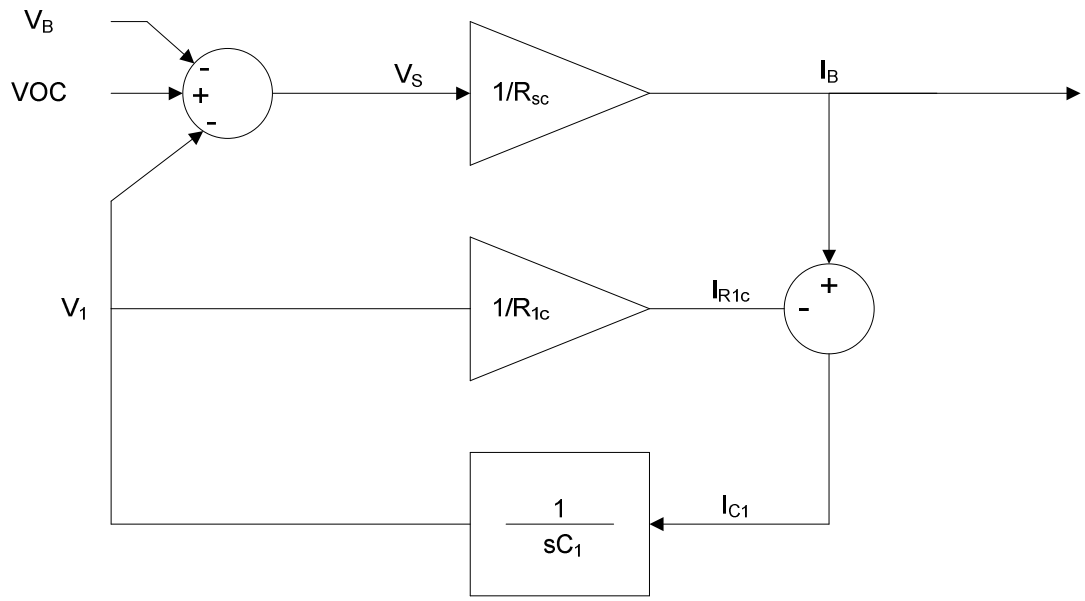

Figure 2.16: Block diagram of battery equivalent circuit for charging process

The equations driven from the block diagram are as follows:

$$V_s = VOC - V_B - V_1 \quad \textbf{(2.1)}$$

$$I_B = \frac{V_s}{R_{sc}} = I_{C1} + I_{R1c} \quad \textbf{(2.2)}$$

$$I_{R1c} = \frac{V_1}{R_{1C}} \quad \textbf{(2.3)}$$

$$V_1 = I_{C1}\frac{1}{sC_1} \quad \textbf{(2.4)}$$

C_1 is a constant capacitance whose value is 250mF. The sum of the resistances R_{1C} and R_{SC} represents the charging internal resistance of the battery and their values are equal, therefore:

$$R_{SC} = R_{1C} = R_C \quad \textbf{(2.5)}$$

By using these equations the relationship between the battery voltage and battery current is derived as follows:

$$I_B(s) = \left(VOC - V_B(s)\right)\frac{1}{R_C}\frac{s + \dfrac{1}{R_C\ C_1}}{s + \dfrac{2}{R_C\ C_1}} \quad \textbf{(2.6)}$$

As stated in Section 1.2.2.2 and Section 1.2.2.5 and shown in Figure 1.10 and Figure 1.13 open circuit voltage and internal resistance are dependent on SOC.

Note that, in Equation (2.6) the sign of resultant battery current is negative. This is because, with the negative signed charging current, the charge of energy, E_{cd}, which is calculated by the algorithm given in Figure 2.7, is negative. Therefore the energy left, E_L is going to increase signifying the charge up of the battery.

If SOC was regarded as an input of the transfer function, then the system would be multi-input single-output system, where the inputs were the battery voltage (V_B), state-of-charge (SOC) and the output was the battery current (I_B). So, the general form of the transfer function would be as follows:

$$I_B(s) = G_1(s)SOC(s) + G_2(s)V_B(s) \quad \textbf{(2.7)}$$

Assume that the relationship between the open circuit voltage, internal resistance and the state-of-charge was linearized and expressed as a transfer function. Then VOC and R_C, given in Equation (2.6), could be written with their own transfer functions:

$$\frac{VOC(s)}{SOC(s)} = G_{11}(s) \quad \textbf{(2.8)}$$

$$\frac{R_C(s)}{SOC(s)} = G_{22}(s) \quad \textbf{(2.9)}$$

If Equation (2.8) and Equation (2.9) were implemented within the main transfer function, then Equation (2.6) would be:

$$I_B(s) = \left(G_{11}(s)SOC(s) - V_B(s)\right)\frac{1}{G_{22}(s)SOC(s)}\frac{s + \dfrac{1}{G_{22}(s)SOC(s)C_1}}{s + \dfrac{2}{G_{22}(s)SOC(s)C_1}} \quad \textbf{(2.10)}$$

However, it is not possible to linearize Equation (2.10) and derive a multi-input single-output system as shown in Equation (2.7) or to linearize the relationship

between VOC, R_C, SOC and to derive proper transfer functions as shown in Equation (2.8) and Equation (2.9). In order to linearly analyze the model, therefore, the transfer function of the battery model should be analyzed as a single-input single-output system, where the open circuit voltage, the pole, zero and gain of the transfer function are evaluated for a given value of SOC.

As a result Equation (2.6) should be rewritten as follows:

$$I_B(s) = \left(G_{11}(s)SOC(s) - V_B(s)\right)\frac{1}{G_{22}(s)SOC(s)}\frac{s + \dfrac{1}{G_{22}(s)SOC(s)C_1}}{s + \dfrac{2}{G_{22}(s)SOC(s)C_1}} \qquad \textbf{(2.11)}$$

Equation (2.11) shows that the battery current is negative; therefore the battery is going to be charged, when the battery voltage, V_B is greater than the open circuit voltage. The change of the current varies with the internal resistance, therefore SOC. The change of gain, zero and pole of the transfer function is shown in Figure 2.17. The change of open circuit voltage as a function of SOC is also shown in Figure 2.18.

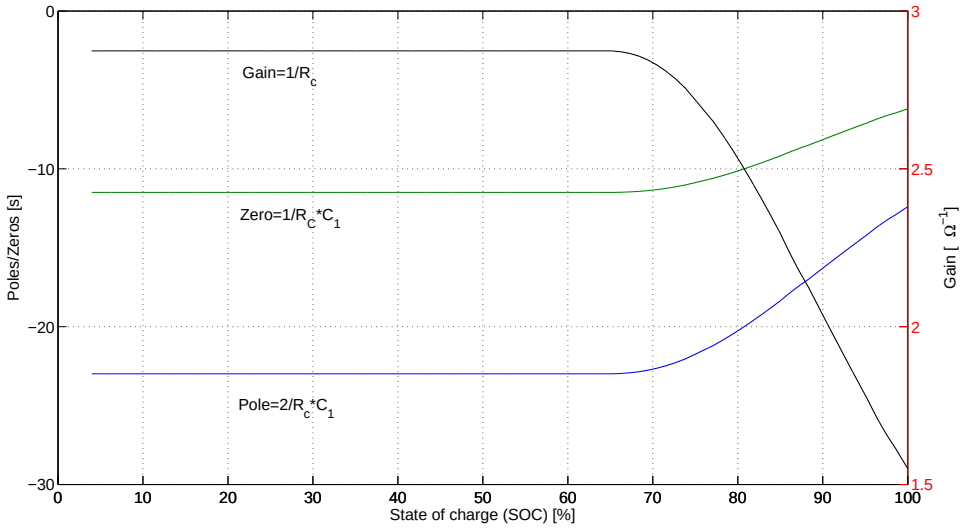

Figure 2.17: Change of gain, zero and pole of battery charging transfer function

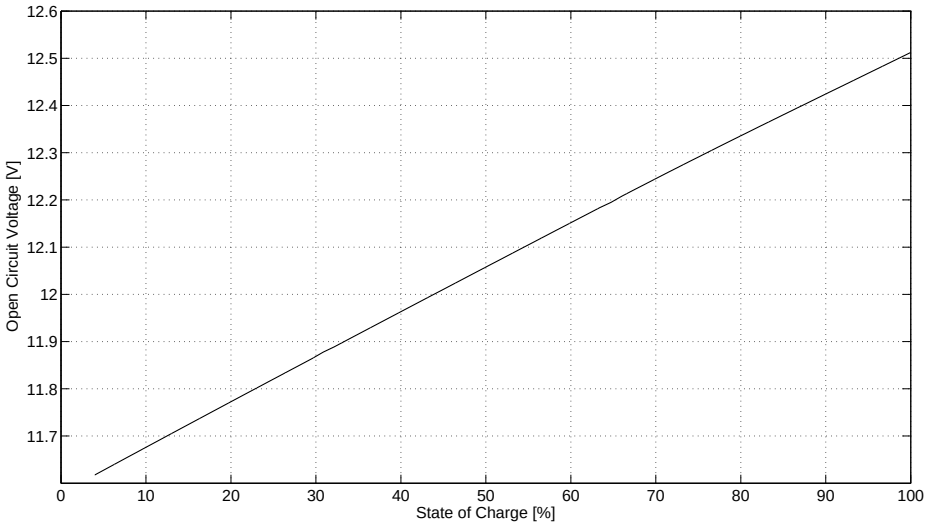

Figure 2.18: Open circuit voltage-SOC characteristic of lead-acid battery model

2.4.1.2 Discharging Transfer Function

Discharging characteristics of the battery model have been derived by monitoring the battery voltage at different current rates. In contrast to the charging model, discharging model should express the change of output voltage under a specific discharge current and SOC. The block diagram of equivalent circuit for discharging process is shown in Figure 2.19.

Following the same method used in Section 2.4.1.1 the relationship between the battery current and battery voltage is derived as follows:

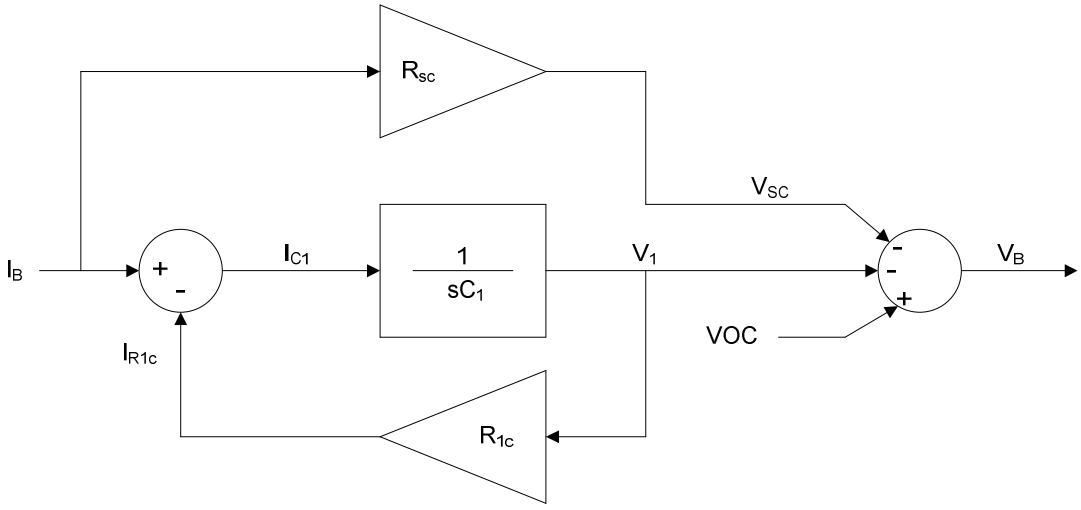

Figure 2.19: Block diagram of equivalent circuit for discharging process

$$V_B(s) = VOC_{(SOC)} - I_B(s) \cdot R_{D(SOC)} \left(\frac{s + \frac{2}{R_{D(SOC)} \cdot C_1}}{s + \frac{1}{R_{D(SOC)} \cdot C_1}} \right) \quad \textbf{(2.12)}$$

Equation (2.11) and Equation (2.12) state that the transfer function derived for the charging process represents the admittance of the battery, whereas the discharging process represents the impedance. These findings conclude that the impedance of the battery is characterized with the discharging resistance and the admittance with the charging resistance.

3. PERMANENT MAGNET SYNCHRONOUS ALTERNATOR

The number of electrical loads even in a conventional vehicle is increasing rapidly, with the use of many electrically powered systems, such as power windows, power steering, power brakes and so on. This ends up with the need of a vehicle electrical system with high efficiency and high power density, where low fuel consumption and exhaust emissions should also be considered.

In the automotive industry the Lundell-type machine, which was described in detail in Section 1.1, has been used for years, but the increasing power demand is close to the capability limits of the Lundell technology [10]. Thus, in a few years, it will not be possible to handle the increased loads with Lundell-type machine especially at idle speeds.

3.1 Vehicle Alternator Trends

As stated in [4], Lundell-type machine is commonly used because of its relatively long operational life and its claw-pole rotor design, which makes it easy to produce with low manufacturing costs. But its efficiency is low especially at low speeds and the output power is limited.

In [4] some other electrical machine technologies to be used as alternator in automotive application were compared:

Lundell Type:

- Comparatively low cost
- Relatively easy to manufacture
- Acceptable operational life
- Low efficiency
- Limited in output power

- Approaching the end of its life cycle due to its power limitations and the effect of its low efficiency on fuel consumption
- High rotor inertia tends to aggravate belt slip

DC Generator:

- Not expensive
- Efficiency is not better than the Lundell type
- High length to diameter aspect ratio
- Commutator and brushes must carry full output current
- Armature speed is limited by inability to retain the windings
- Requires more maintenance than Lundell type due to higher brush wear
- Use of a cutoff relay or semiconductor to prevent discharging the battery through the generator
- Housing the regulator inside the machine will be a challenge

Induction Alternator:

- A reactive power source should be used for the excitation current
- Efficiency will be higher than the Lundell type
- Stator will be similar to the Lundell type in design and manufacture
- Rotor will be laminated with an aluminum squirrel cage cast into the slots
- Inertia can be lower than the Lundell permitting more power to be generated without belt slip
- Length to diameter ratio is not as limited as the Lundell type so power can be increased to some degree by increasing the length but not diameter

Switched Reluctance Alternator:

- Efficiency will be higher than Lundell type
- Brushless

- Stator will be similar to the Lundell type in design and manufacture
- Rotor is solid steel with poles
- Inertia can be lower than the Lundell type permitting more power to be generated without belt slip
- Length to diameter ratio is not limited as the Lundell type so power can be increased to some degree by increasing length but not diameter
- Would create more noise than induction alternator

3.2 Permanent Magnet Synchronous Machine

3.2.1 Properties of Permanent Magnet Synchronous Machine as Alternator

Permanent magnet synchronous machine (PMSM) offers many advantages as a vehicle alternator. These advantages were discussed in [11] and compared with Lundell-type machine:

The output power of PMSM is greater than the Lundell-type machine for the same speed and volume, because its reactance is lower due to the low permeability of the permanent magnet material compared with iron. PMSM can achieve an optimum level of airgap flux density with a relatively thin magnet mounted on the hollow, lightweight rotor, whereas Lundell-type machine requires more field ampere turns to reach this flux density, because of its inefficient rotor magnetic circuit. But the space available for the field coil is limited to achieve these ampere turns, because the ability to dissipate the heat generated becomes an important restriction.

Because the flux path per pole is completed within a radial plane, the need for an axial flux carrier in a PMSM is eliminated, such as the steel shaft and core in Lundell-type machine, which have to be sized to carry the entire flux of all poles. Also the field coil, slip rings and brushes are eliminated, resulting a lightweight, maintenance-free and compact machine [11].

In a PMSM the magnetic field is produced by the magnets, which results in a relatively lower rotor copper loss. The rotor surface is smoother, which, as a result, produces less windage loss and less windage noise as compared with claw-pole configuration of Lundell-type machine. Due to low magnetic permeability of the magnets, the loss at pole face, caused by stator slotting is less than that of the

Lundell-type machine in the solid steel poles. With the use of powerful magnets, it is possible to design a PMSM with optimum flux level, due to its effective magnetic circuit. As a result the required voltage can be generated with lower number of stator winding turns, which, thereby, means lower stator copper loss. Unlike the Lundell-type machine, length-to-diameter ratio is not limited; therefore, it is possible to increase the efficiency in PMSM with a longer machine if the machine diameter is constrained by the space available [11].

The simple rotor construction of PMSM has a much lower inertia than the one of a Lundell-type machine. Also, a high degree of manufacturing flexibility can be provided by the nature of its two-dimensional radial magnetic flux path. Therefore, different machine ratings for different vehicles can be achieved by varying the machine length at the same diameter.

Although overall manufacturing cost of PMSM, because of control electronics and assembly, will be higher than induction, switched-mode reluctance and Lundell-type machine. It is possible to reduce it by minimizing the manufacturing tolerances, because PMSM is less sensitive to airgap variations due to its low magnet permeability. Low magnet permeability also reduces the magnetic noise considerably, particularly under load [11].

3.2.2 Comparison between Lundell-Type Machine and Permanent Magnet Synchronous Machine

In [12] an electrically magnetized synchronous machine (EMSM) without slip rings was proposed and its performance was compared with a radial PMSM of similar form and size.

It was identified that PMSM of similar size delivered %17 more torque, but %42 higher current. Torque to weight ratio was calculated as 1.06 Nm/kg for EMSM, whereas 1.78 Nm/kg for PMSM. It was also stated that the torque ripple in PMSM was four times and the leakage %16 smaller than in the electrically magnetized synchronous machine. Table 3.1 shows the weight comparison of machine components. It was shown that PMSM is lighter than EMSM.

Table 3.1: Weight Comparison between Electrically Magnetized Synchronous Machine and Permanent Magnet Synchronous Machine [12]

Component	Electrically Magnetized Synchronous Machine	Permanent Magnet Synchronous Machine	Difference (%)
Stator yoke	34.5 kg	25.2 kg	26.95
Rotor	11.5 kg	22.6 kg	-96.52
End-plates	31.7 kg	3.0 kg	90.50
Stator coils	14.9 kg	18.7 kg	-25.50
Rotor coils	9.4 kg	-	-
Magnets	-	1.9 kg	-
Shaft	6.4 kg	6.4 kg	0.00
Total	108.4 kg	77.8 kg	28.22

Regarding these findings PMSM can be a long term solution for the increasing electrical load demands of automotive industry with a better efficiency and without increasing fuel consumption and weight. In this study PMSM is used for the electricity generator of the system.

PMSM is typically constructed with the magnets attached to the rotor, and a three phase winding in the stator core. As stated in Section 1.1.1, the output voltage of a Lundell-type machine varies with speed and excitation current, which is adjusted due to load demand. In PMSM the conductance of the magnet is poor that the flux produced by the stator currents does not induce voltage on the magnets. So the mutual inductance between stator and the magnet, thus the magnet current is zero. Therefore, permanent magnets can be modeled as a constant flux linkage source with constant value [13]. As a result the output voltage of PMSM is directly dependent on speed.

There are mainly two kinds of PMSM: for a saliency ratio of unity, the machine is called surface mounted permanent magnet. For a saliency ratio exceeding two, the machine is called interior permanent magnet machine, in which embedded magnets are used as shown in Figure 3.1. Since the interior permanent magnet machine is a type of salient-pole synchronous machine, each of the d- and q- axes equivalent

circuits is characterized by a different value of stator inductance, L_d and L_q respectively. One of the features that sets the interior permanent magnet machine apart from classic wound-field salient pole synchronous machine (such as Lundell-type machine) is the fact that the d-axis inductance in interior permanent magnet machine is less than that of the orthogonal q-axis, because of the low magnetic permeability of the permanent magnets [14]

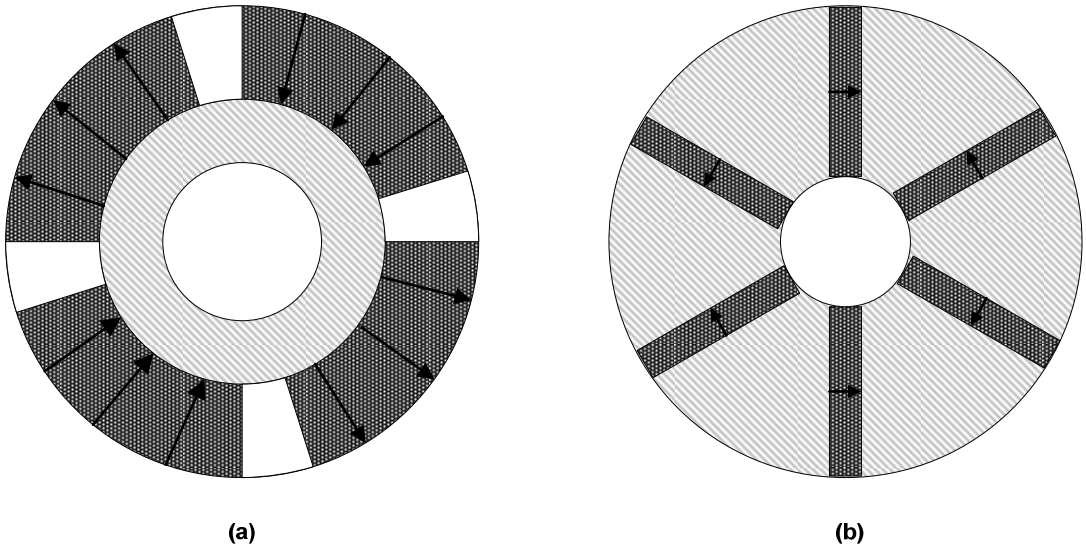

Figure 3.1: (a) Surface Mounted Permanent Magnet Machine (b) Interior Permanent Magnet Machine [15]

3.2.3 Characteristics of Permanent Magnet Synchronous Alternators

In [16] the feasibility and application of PMSM in a stand-alone electricity generation system was reviewed. Also, modeling of permanent magnet synchronous machines is analyzed in [13].

The permanent magnets should efficiently be used in such a structural design that the operating point of the magnetic material (i.e. flux density) and magnetic field strength are at their maximum energy production points. For a particular airgap and magnet geometry the flux density, B_m and the field strength, H_m in the magnet are related by:

$$\frac{B_m}{H_m} = -\mu_0 \frac{a_g l_m}{a_m l_g} \qquad \textbf{(3.1)}$$

In case of magnets mounted adjacent to the air gap, as in surface mounted permanent magnet machines, air gap area, a_g and the magnet cross section area, a_m are equal.

But for embedded magnets, as in interior permanent magnet machines, they are in general not similar.

Equation (3.1) thus defines the path of loading which represents the operating point. The operating point is the intersection of the load line and the demagnetization recoil line which is shown for Alnico 5 and samarium-cobalt magnets in Figure 3.2. It is an effective design when the intersection is on the maximum energy hyperbola for the particular magnet material.

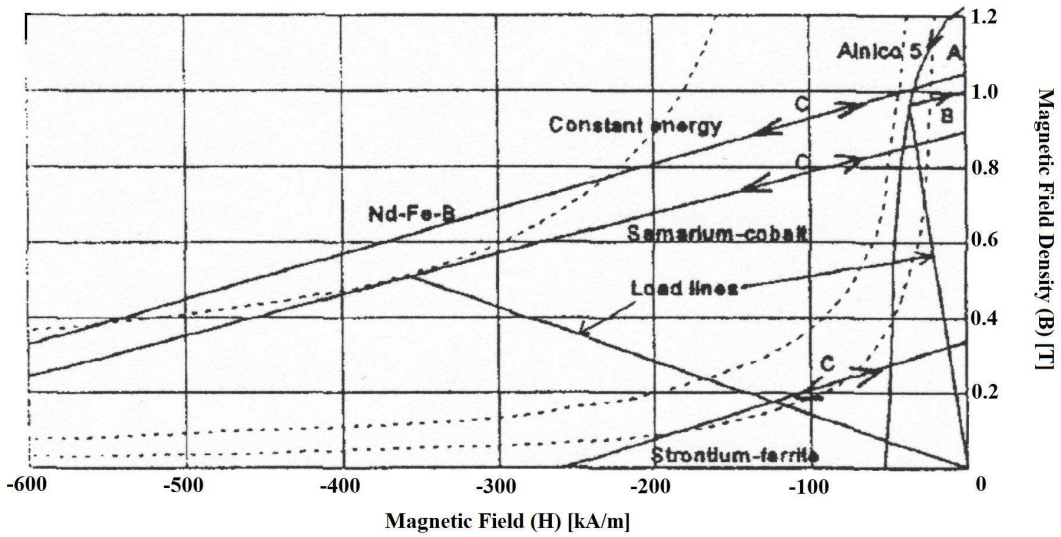

Figure 3.2: Second quadrant demagnetization characteristics of a few permanent magnet materials [16]

The relative magnitude of the synchronous reactance is also different in surface mounted and interior permanent magnet machines [16]. In the surface mounted machine, the stator winding has appreciably more leakage inductance, due to the relatively low reluctance afforded by the steel at both sides of the air gap.

4. SWITCHED-MODE RECTIFIER

As discussed in Chapter 3 permanent magnet synchronous machine can be a long term solution for supplying the increasing electrical power demand of the automotive industry. The voltage regulation to compensate of speed and load variations for Lundell-type machine is not applicable for permanent magnet synchronous machine, because in contrast to Lundell-type machine the excitation current in PMSM is produced by the magnets attached to the rotor surface, therefore a simple control by means of adjusting the field current is not possible.

4.1 Control by Split Armature Windings and Two SCR Bridges

In [11] split armature windings and novel electronic voltage regulation scheme were proposed. The system consists of split stator windings with the tap 1/3 the turns. Each of the two three-phase windings sets is connected to a separate phase-controlled silicon-controlled rectifier (SCR) bridge to regulate the alternator variable output voltage (Figure 4.1).

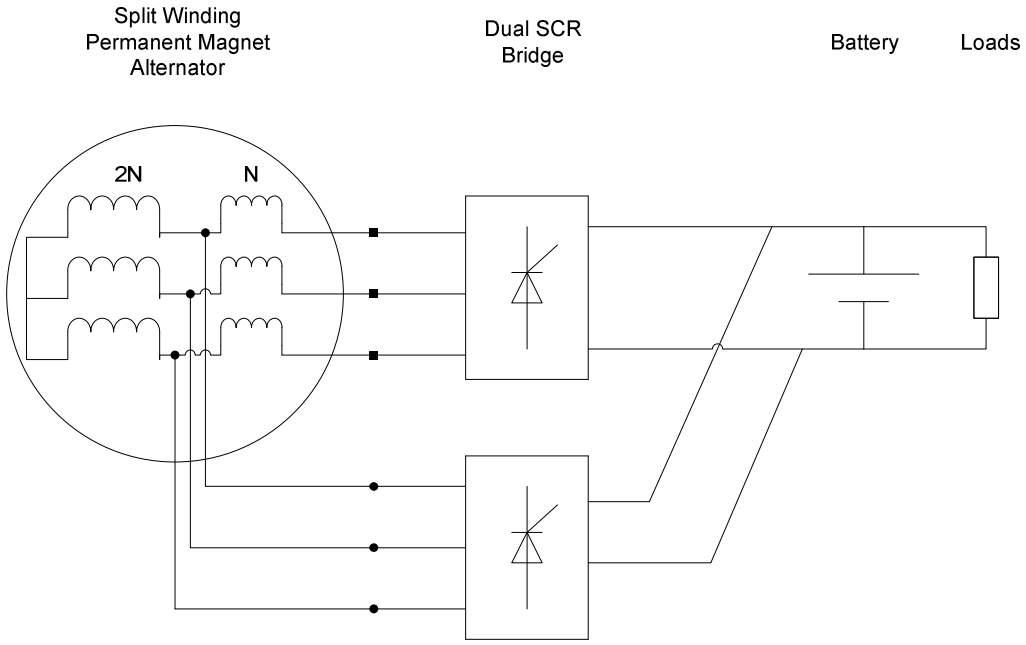

Figure 4.1: Split armature winding system

In this system, the SCR bridge connected to the winding set with higher number of turns is activated to control the output voltage from engine idle speed (n_i) to a speed $n_1=3n_i$. Above n_1, the output voltage of the bridge connected to the winding set with lower number turns is sufficiently high to provide the system voltage. Therefore this bridge is activated while deactivating the other bridge simultaneously. After switching, the current flows through only 1/3 of the stator winding, thus producing only one-third of the copper loss.

Although this proposed system has advantages, such that the stator currents are less pulsed and generating less heat, due to the fact that the speed range covered by each SCR bridge is approximately 3:1, it brings manufacturing costs and control complexity. The stator should be designed for a split winding and this means higher manufacturing costs for the permanent magnet alternator. Besides, the power electronic block should contain 12 SCR switches and the firing pulses to control the output voltage should be maintained by a phase-lock-loop generator. This will increase the cost and complexity of the control system.

In many studies published in near past, switched mode rectifier (SMR) has been proposed for the output voltage regulation of PMSM. In this chapter, the properties and characteristics of SMR are going to be analyzed. Also its added value to the performance of PMSM is going to be investigated.

4.2 Properties and Characteristics of Switched-Mode Rectifier

The switched-mode rectifier consists of a three-phase rectifier, a single PWM controlled switch, a diode and a capacitor (Figure 4.1) and is similar to DC step-up converter in operation.

With a high frequency switching and sufficiently large machine inductance, the alternator sees only the time-average effect of the PWM switching; hence a regulated DC output voltage is produced, which is dependent on the duty-cycle [17].

SMR utilizes a fault mode of inverter driven permanent magnet synchronous motor, which is called uncontrolled generation. This fault mode was discussed in [14].

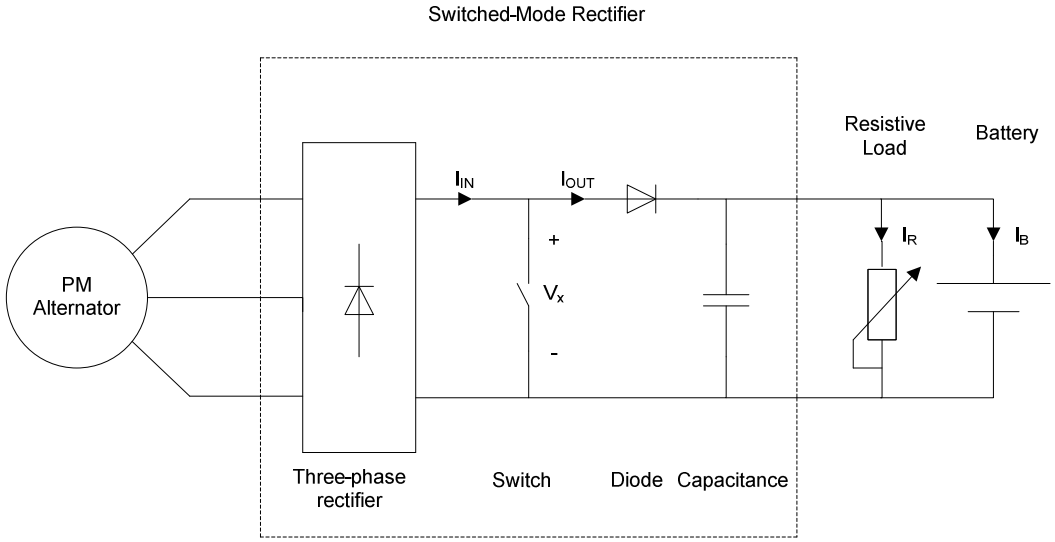

Figure 4.2: Switched-mode rectifier

4.2.1 Uncontrolled Generation in Inverter Driven PMSM

When used as motor, PMSM is driven by three-phase inverters, which is fed through a DC supply as shown in Figure 4.3. In this drive configuration, the amplitude of the line-to-line back-EMF generated by the spinning interior permanent magnets may significantly exceed the DC supply voltage when machine is rotating over a certain speed, at which the speed range for constant-power operation mode begins (Figure 4.4) [14].

Such high speed operation poses no problem as long as the inverter switches are operating properly in their controlled flux-weakening mode, since maximum

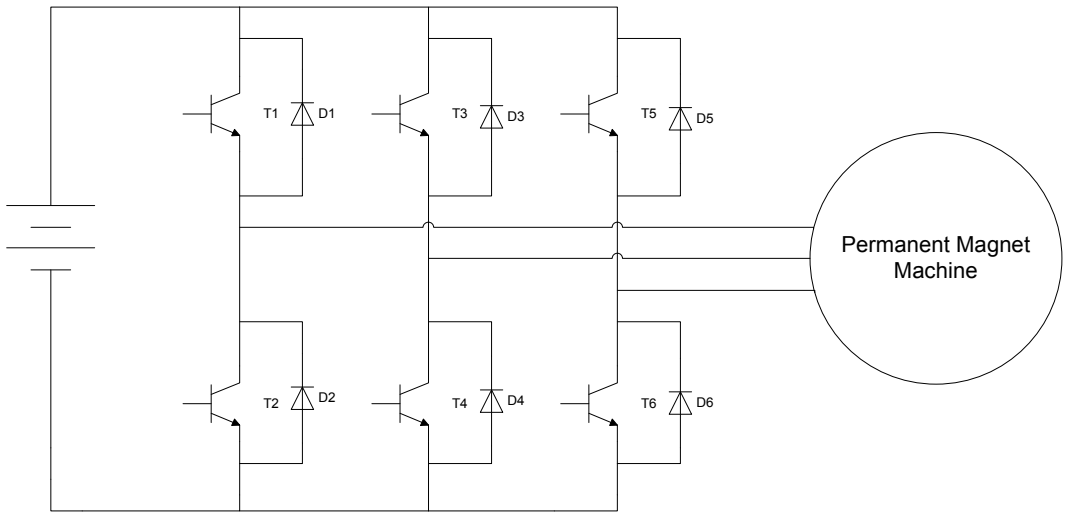

Figure 4.3: Inverter driven permanent magnet synchronous motor

machine terminal voltage is automatically limited by the applied DC supply voltage. If a fault arises under these high-speed operating conditions by suddenly removing the gate signals from all of the controlled inverter switches, which causes the inverter to shut down, the high amplitude of the machine back-EMF source causes current to flow back to the DC-link until the rotor speed is reduced sufficiently to extinguish the current flow. Therefore, PMSM acts as a generator immediately after this shutdown and free-wheeling diodes behave as an uncontrolled bridge rectifier. Interior permanent magnet machines whose saliency ratio is greater than two as discussed in Section 3.2, are vulnerable to operating in this uncontrolled generator mode whenever the rotor speed is above a value at which the line-to-line back-EMF of the machine equals to the DC-link voltage. [14].

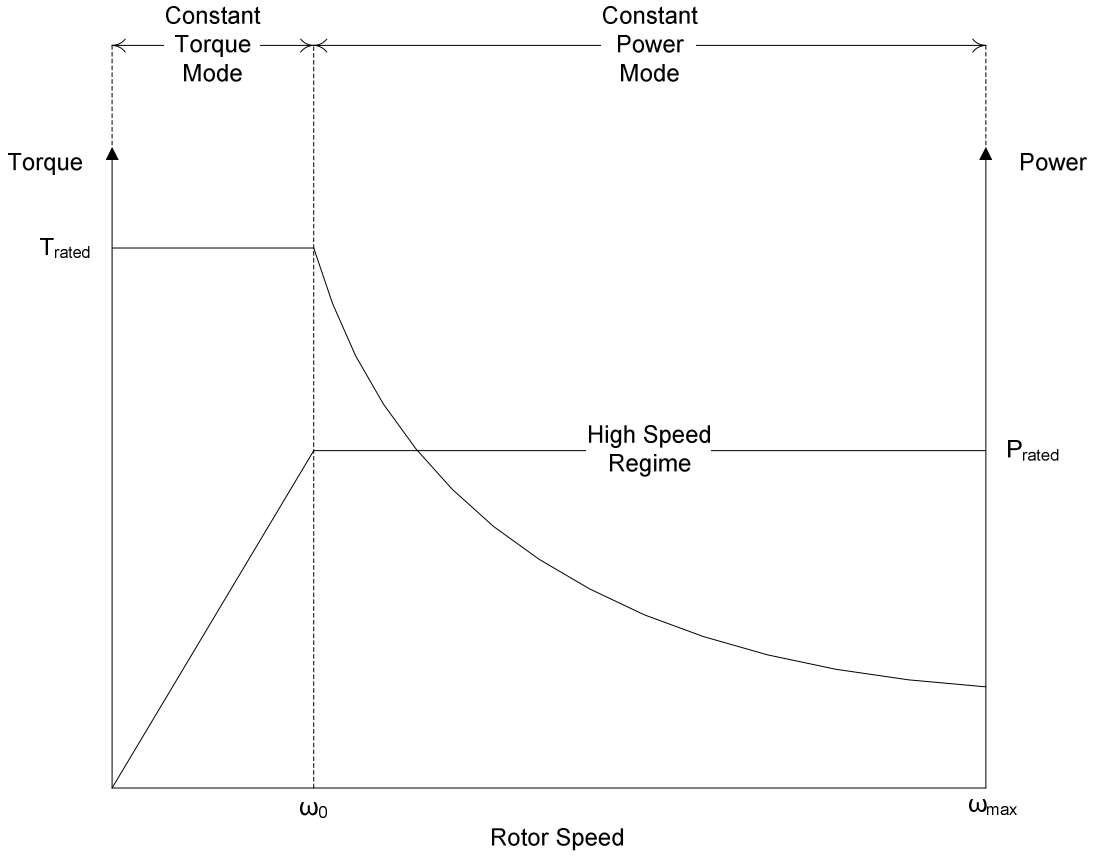

Figure 4.4: Operation modes of PMSM as motor

4.2.2 Relationship between Switched-Mode Rectifier and PMSM

Uncontrolled generation mode of PMSM signifies a relationship between the saliency ratio and the performance of the alternator. This relationship was discussed in [18]. Figure 4.5 shows the output current and power versus output voltage curves of permanent magnet machines with different saliency ratios when connected to a

three-phase resistive load. As mentioned in Section 3.2 for a saliency ratio of unity, the machine is called a surface permanent magnet machine and its equivalent circuit is a voltage source with a series reactance. Therefore, when the circuit is solved for a resistive load, the output voltage-current curve becomes a semi-circle. But as the saliency ratio is increased, the maximum output power increases significantly. For saliency ratio exceeding two, the curve develops an increasing voltage overshoot and the output voltage under load becomes higher than the open-circuit voltage. This characteristic of interior PMSM is because of the bistable and hysteresis effect during uncontrolled generation [14, 18]

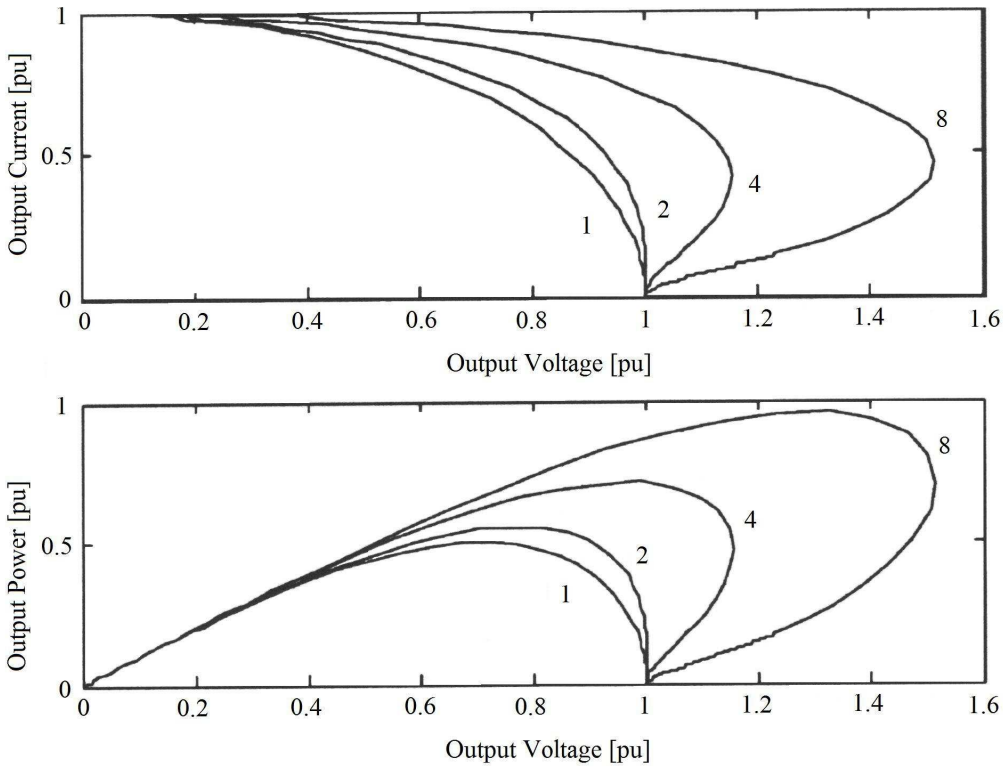

Figure 4.5: Output voltage-output current/output power characteristics of permanent magnet synchronous machine with different saliency ratios [18]

Figure 4.6 shows the same curve for different speeds, simulated with the permanent magnet synchronous machine model with a saliency ratio of 6. The parameters of machine model are given in Table 4.1. The voltage-current curve, which was measured at different resistive loads, varies significantly with speed.

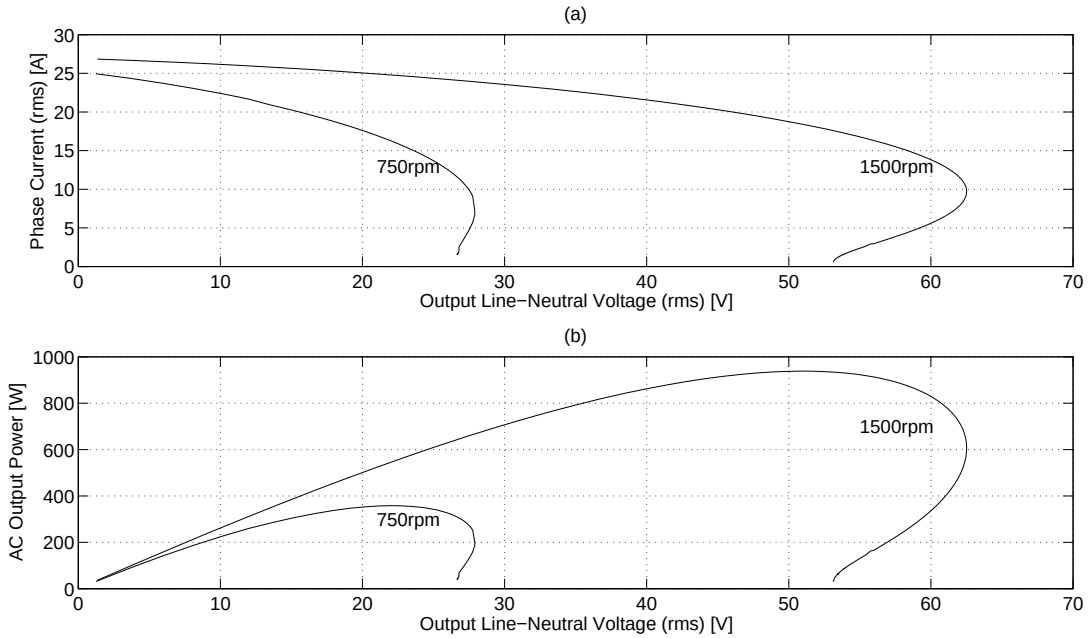

Figure 4.6: Output voltage-output current/output-power characteristics of an interior permanent magnet synchronous machine at 750 rpm and 1500 rpm

For a saliency ratio greater than two, permanent magnet synchronous machine is a salient pole synchronous machine. Therefore, circuit equation for the stator circuit is:

$$\overline{V}_t = \overline{E}_f + \overline{E}_d + \overline{E}_q - R_a \bar{I}_a \quad \textbf{(4.1)}$$

$$\overline{E}_d = -jX_d \bar{I}_d \quad \textbf{(4.2)}$$

$$\overline{E}_q = -jX_q \bar{I}_q \quad \textbf{(4.3)}$$

$$\bar{I}_a = I_q - jI_d \quad \textbf{(4.4)}$$

When the alternator is short circuited, as in the case of SMR, output voltage of the machine, V_t is zero. Therefore,

$$\overline{E}_f = -\left(\overline{E}_d + \overline{E}_q\right) + R_a \bar{I}_a \quad \textbf{(4.5)}$$

Substituting Equation (4.2), (4.3) and (4.4) into Equation (4.5):

$$\bar{E}_f = R_a\bar{I}_a + jX_d\bar{I}_d + jX_q\bar{I}_q \quad \textbf{(4.6)}$$

Figure 4.7 shows the phasor diagram for a short circuited machine, where armature current, I_a lags the induced voltage, E_f by 90^0.

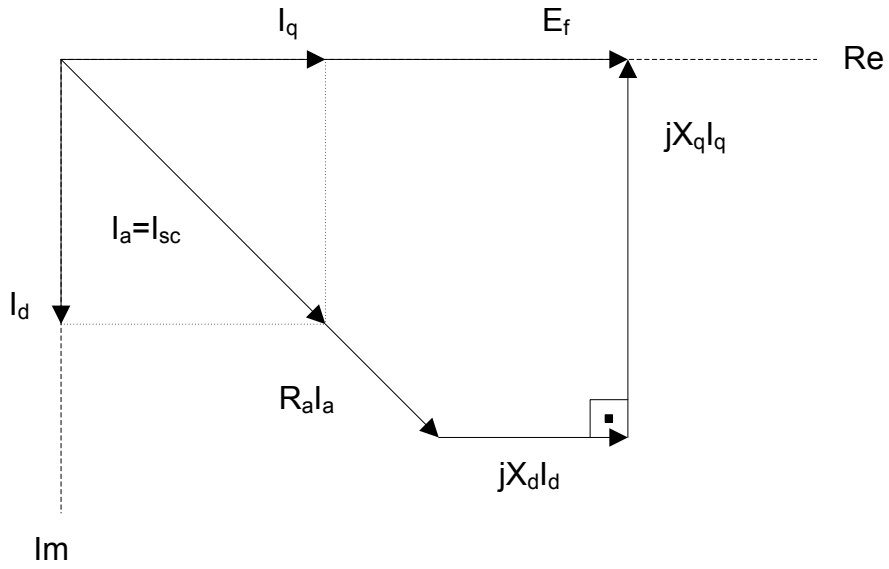

Figure 4.7: Phasor diagram for short circuited salient-pole synchronous machine

From the phasor diagram:

$$\bar{E}_f = E_f + j0 \quad \textbf{(4.7)}$$

$$\bar{I}_a = I_q - jI_d \quad \textbf{(4.8)}$$

$$\bar{I}_d = -jI_d \quad \textbf{(4.9)}$$

$$\bar{I}_q = I_q \quad \textbf{(4.10)}$$

Substituting Equation (4.7), (4.8), (4.9) and (4.10) into Equation (4.6):

$$E_f + j0 = \left(X_d I_d + R_a I_a\right) + j\left(X_q I_q - R_a I_d\right) \quad \textbf{(4.11)}$$

Therefore, from Equation (4.11):

$$E_f = X_d I_d + R_a I_a \quad \textbf{(4.12)}$$

$$0 = X_q I_q - R_a I_d \quad \textbf{(4.13)}$$

If Equation (4.12) and (4.13) are solved for I_d and I_q :

$$I_d = \frac{E_f}{R_a^2 + X_d X_q} X_q \quad \textbf{(4.14)}$$

$$I_q = \frac{E_f}{R_a^2 + X_d X_q} R_a \quad \textbf{(4.15)}$$

As a result, short circuit current can be calculated by using Equation (4.14) and (4.15):

$$I_{sc} = I_a = \sqrt{I_d^2 + I_q^2} = \frac{E_f}{R_a^2 + X_d X_q} \sqrt{R_a^2 + X_q^2} \quad \textbf{(4.16)}$$

Substituting values for R_a, X_d, X_q and E_f into Equations (4.16) short circuit current can be calculated analytically:

$$I_{sc} = \frac{\frac{92.4}{\sqrt{3}}}{0.77^2 + \left(2\pi 50\ 6.15\ 10^{-3}\right)\left(2\pi 50\ 36.2\ 10^{-3}\right)} \sqrt{0.77^2 + \left(2\pi 50\ 36.2\ 10^{-3}\right)^2} \quad \textbf{(4.17)}$$

The result is 26.97A and is very close to the one given in Table 4.1. The induced voltage, E_f and synchronous reactances, X_d, X_q can be rewritten as a function of alternator mechanical angular speed:

$$E_f = k_e \omega_m \quad \textbf{(4.18)}$$

$$X_d = p \omega_m L_d \quad \textbf{(4.19)}$$

$$X_q = p \omega_m L_q \quad \textbf{(4.20)}$$

By substituting Equations (4.18), (4.19) and (4.20) into Equation (4.16), short circuit current as a function of alternator speed can be driven:

$$I_{sc} = k_e \frac{\sqrt{R_a^2 \omega_m^2 + p^2 L_q^2 \omega_m^4}}{R_a^2 + p^2 L_d L_q \omega_m^2} \quad \textbf{(4.21)}$$

By using Equation (4.21), the change of rms value of short circuit current with respect to alternator speed is calculated and shown in Figure 4.8. It is obvious from the figure that, short circuit current is nearly constant especially over the rated synchronous speed.

Table 4.1: Parameters for Permanent Magnet Synchronous Machine

Machine Parameter	Value
pole-pairs	2
q-axis inductance (unsaturated) [mH]	36.2
d-axis inductance (saturated) [mH]	6.15
phase resistance (ohm)	0.77
saliency ratio (max)	6
short-circuit current @ 1500 rpm (rms)	26.9
magnet flux (peak) [Wb]	0.24
line-to-line back-EMF @ 1500 rpm (rms)	92.4

Thus if the back-EMF voltage is large compared with the output voltage, then the output current will not be significantly affected by speed and the alternator can be modeled by a constant current source. An alternator with a constant output current can be controlled by a switched-mode rectifier to produce a regulated DC output voltage, where the duty-cycle determines the amount of output current that is fed to the load. [18].

As a result, in order to fully utilize this constant current characteristic and use switched-mode rectifier for voltage regulation, the machine should be designed with a back-EMF voltage which is much larger than the rated output voltage and a short circuit current which is equal to the rated output current. For this kind of machine design the constant power speed range (CPSR) is determined by the back-EMF ratio and saliency ratio, therefore for a given CPSR, increasing the saliency ratio reduces the required value of back-EMF ratio [18].

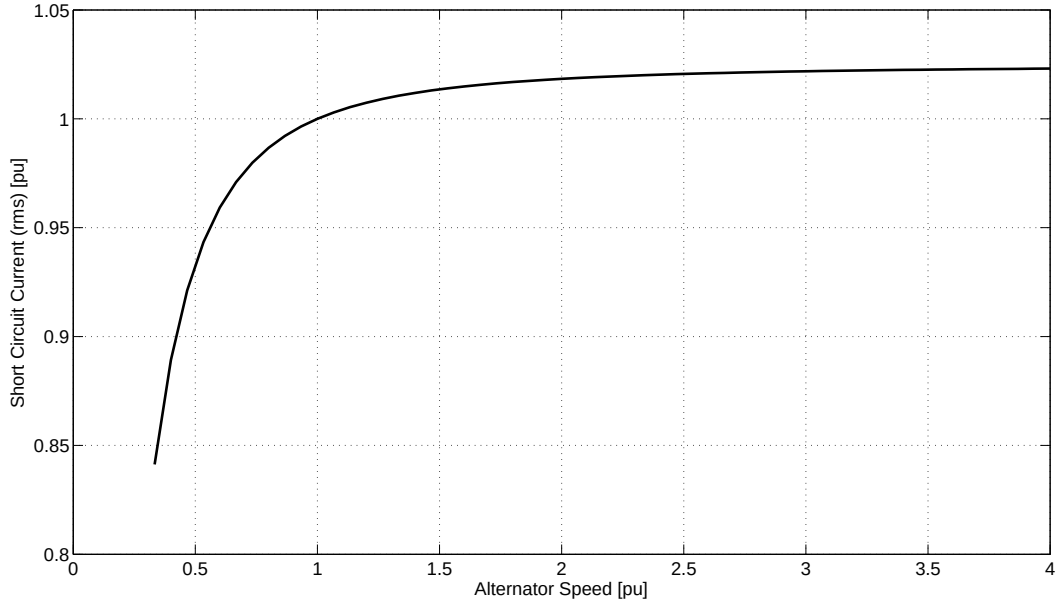

Figure 4.8: Short circuit current as a function of alternator speed

4.2.3 Operational Principles of Switched-Mode Rectifier

As stated in Section 4.2.2 in order to utilize SMR for PMSM the machine should have both high back-EMF voltage and high reactance. For a vehicle electrical system, the duty-cycle of SMR should be adjusted in order to maintain constant output voltage.

The operating mode of the SMR can be divided into two regions dependent on the alternator speed as discussed in [17]. Firstly at high speeds, the alternator back-EMF voltage is much greater than output voltage; hence duty-cycle of the switch controls the output current.

$$I_{OUT} = (1-d)I_{IN} \quad \textbf{(4.22)}$$

Assuming the output voltage is constant, the output power is proportional to I_{OUT}; hence (1-d).

At low speeds, the alternator back-EMF is smaller than DC link voltage. Here the switched-mode rectifier acts as a boost rectifier and allows some output power to be generated. Operation at low speeds can also be explained by describing the effect of the duty-cycle control of the switched-mode rectifier as reducing the effective DC link voltage seen by the alternator [17]:

$$V_X = (1-d)V_{DC} \quad \textbf{(4.23)}$$

The switched-mode rectifier allows the alternator to produce output power at low speeds by operating as a boost rectifier. It allows the output current at all speeds to be controlled by the duty-cycle of the switch.

Figure 4.9 and Figure 4.10 show the change of mean values of input (I_{IN}) and output (I_{OUT}) currents of switched-mode rectifier at different alternator speeds, when loaded with a 14V-rated constant DC voltage source. It is obvious from the figures that, the input current is almost constant at 36A, which is the rectified machine short circuit current, and the output current varies with the duty-cycle of the switch.

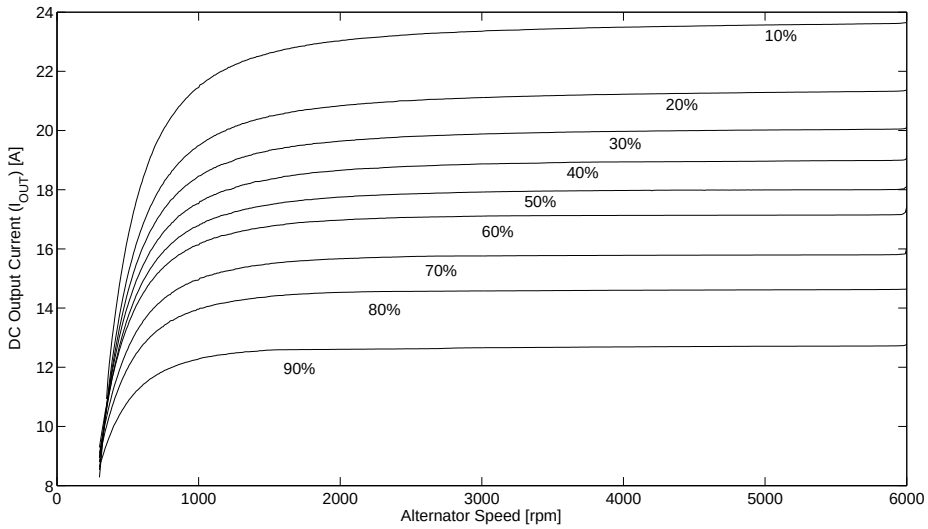

Figure 4.9: Alternator speed-DC output current (I_{OUT}) characteristics at different duty ratios

Stator voltage and current waveforms of the alternator while operating with switched-mode rectifier are shown in Figure 4.11. Although the stator voltage shows the pulse width modulation action of the SMR these high-frequency switching transients are filtered by the large machine inductance, so that the stator current remains sinusoidal [17].

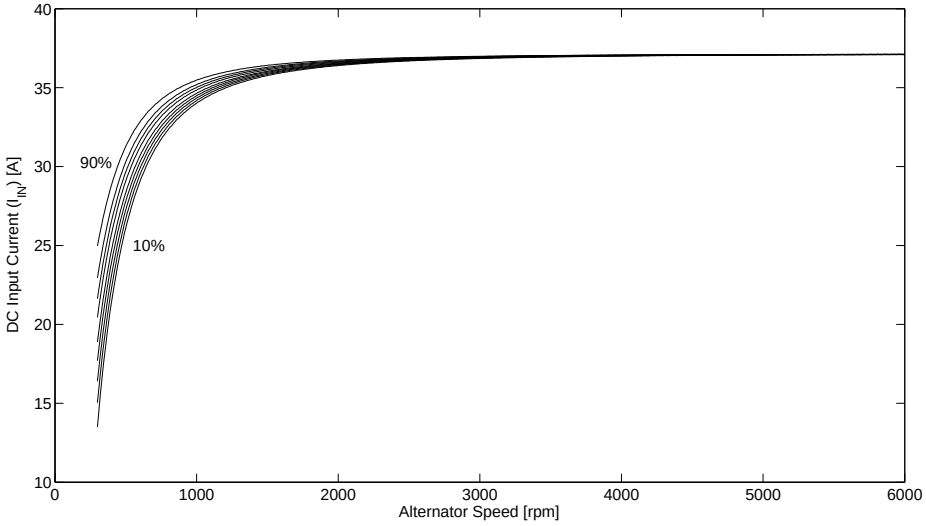

Figure 4.10: Alternator speed-DC input current (I_{IN}) characteristics at different duty ratios

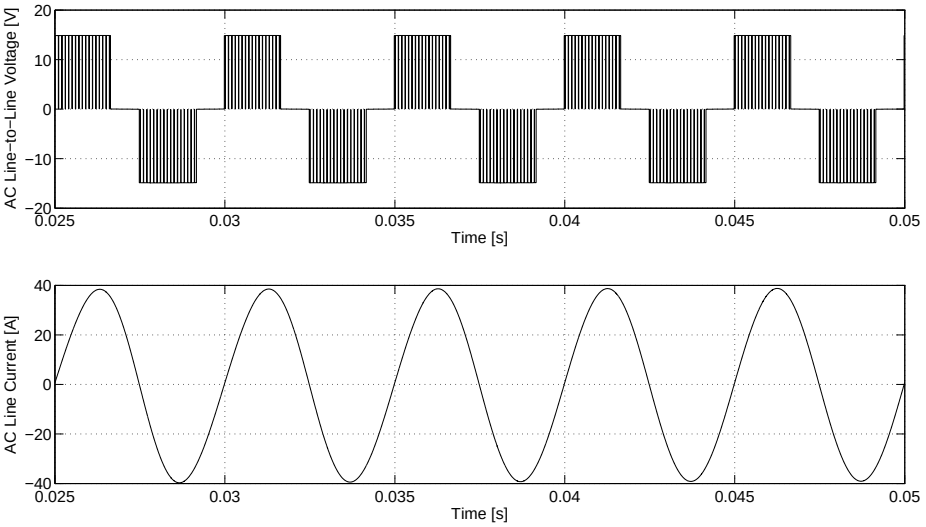

Figure 4.11: Stator voltage and current waveforms of PMSM with SMR at 6000 rpm and 10% duty ratio

5. SIMULATION AND CONTROL OF VEHICLE ELECTRICAL SYSTEM

The task of the vehicle electrical system is to keep the system voltage constant due to load conditions when the engine is running and to maintain the proper charging of the lead-acid battery. The voltage regulation in a conventional vehicle electrical system has been described in Section 1.1.1.

In this study, a permanent magnet synchronous machine, whose properties and characteristics have been described in Chapter 3, is selected as the vehicle alternator and a switched-mode rectifier, whose characteristics and advantages has been discussed in Section 4.1, as the voltage regulator.

Also, as stated in Section 1.2, lead-acid battery is an integral part of the vehicle electrical system. Therefore, it has to be taken into account in the complete system modeling. In [3] a vehicle electric power system simulation, which contains the battery, has been proposed and characteristics of electric power system, electrical load demands and driving environment have been investigated. But in this study, the alternator model belongs to a Lundell-type alternator and the output voltage of the alternator is regarded as it has already been regulated. In [20] a closed-loop output voltage regulation of PMSM has been proposed and designed, but battery has not been considered in the open-loop analysis of the vehicle electrical system.

In this chapter the modeling, open-loop characteristics, closed-loop control and simulation of complete vehicle electrical system composed of SMR regulated interior permanent magnet synchronous machine, a lead-acid battery and electrical loads are going to be analyzed.

5.1 Variable Speed Operation of the Alternator

The alternator is driven by an internal combustion engine. The speed of the vehicle, hence the speed of the engine and the torque transferred to the alternator change due to the road and traffic conditions as shown in Figure 1.3. As stated in Section 1.1 and shown in Figure 5.1 the alternator is connected to the internal combustion engine through a constant ratio belt-pulley system.

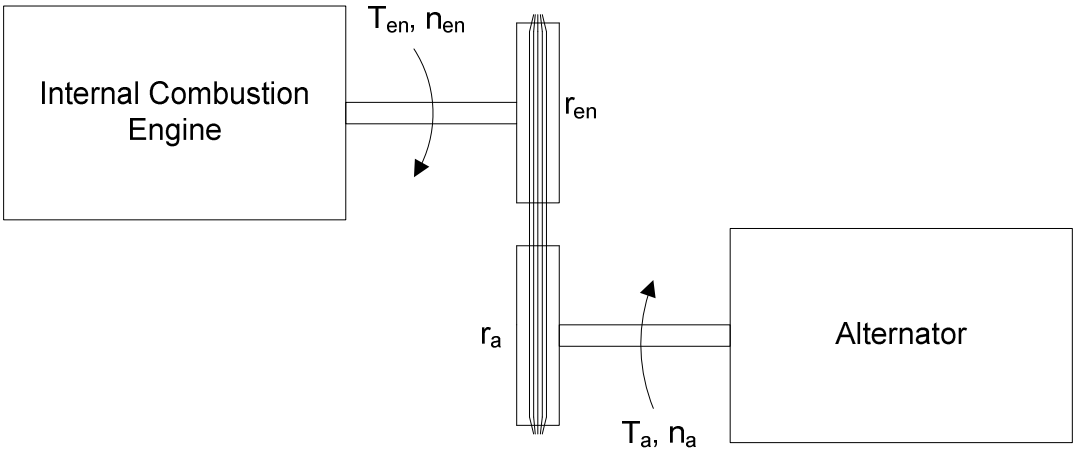

Figure 5.1: Overview of alternator drive mechanics

In order to properly simulate the variable speed operation of the system, models of internal combustion engine and belt-pulley system have been implemented. The internal combustion engine model is a look-up table, which calculates the engine torque due to engine speed and throttle position. The engine map is shown in Figure 5.2.

The belt-pulley system has been modeled by using the relationship between the pulleys and reducing the parameters to the alternator side:

$$\frac{T_{en}}{T_a} = \frac{\theta_a}{\theta_{en}} = \frac{\omega_a}{\omega_{en}} = \frac{r_{en}}{r_a} \qquad \textbf{(5.1)}$$

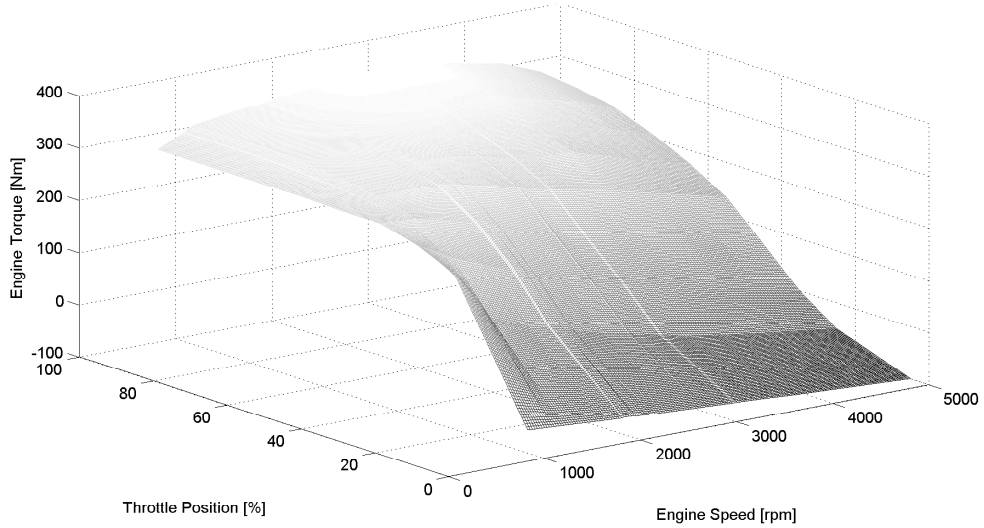

Figure 5.2: Engine map

$$J_{eq} = J_a + \left(\frac{r_a}{r_{en}}\right)^2 J_{en} \quad \textbf{(5.2)}$$

5.2 Open-Loop Characteristics

The proposed system consists of the interior permanent magnet alternator, battery, electrical loads of the vehicle and the switched-mode rectifier. The complete system was shown in Figure 4.2.

I_{IN} represents the rectified machine short-circuit current, I_{OUT} the output current of the switched-mode rectifier, I_C the current flowing through the capacitor, which charges it up and produces the output voltage, I_R the current that flows through the electrical loads of the vehicle and I_B the battery current.

5.2.1 Open-Loop Characteristics of Alternator and Switched-Mode Rectifier

In [20] the detail of closed-loop control of a multiple-barrier interior permanent magnet synchronous machine, whose output voltage is regulated by means of switched-mode rectifier, was discussed. The parameters of the machine were shown in Table 4.1.

In this paper, the output of the switched-mode rectifier was connected to a resistive load and in the open loop tests; a DC voltage source load had been substituted to keep the output voltage constant.

As stated Section 4.2.2 and shown in Figure 4.10, at high speeds the output voltage resembles to the rectified machine short circuit current, $I_{IN,}$ which equals to 36A for the modeled machine (Figure 4.10). Therefore, switched-mode rectifier acts as a current chopper and the output current, I_{OUT} becomes a function of the duty-cycle.

$$I_{OUT} = 36\ (1-d), \quad 0 \le d \le 1 \quad \textbf{(5.3)}$$

In [20] the frequency response of the alternator output current had been measured by subjecting the switched-mode rectifier to sinusoidally-varying duty-cycle command. It had been stated in this article that the gain response, whose measurement values are shown with circles in Figure 5.4, remained flat up to a corner frequency of 600 rad/s and, therefore, the transfer function of the system, given in Equation (5.4), had

been approximated by fitting a second-order response to the measured results. The frequency response of the approximated transfer function is also given in Figure 5.4.

$$G(s) = \frac{1200^2}{(s+1200)^2} \tag{5.4}$$

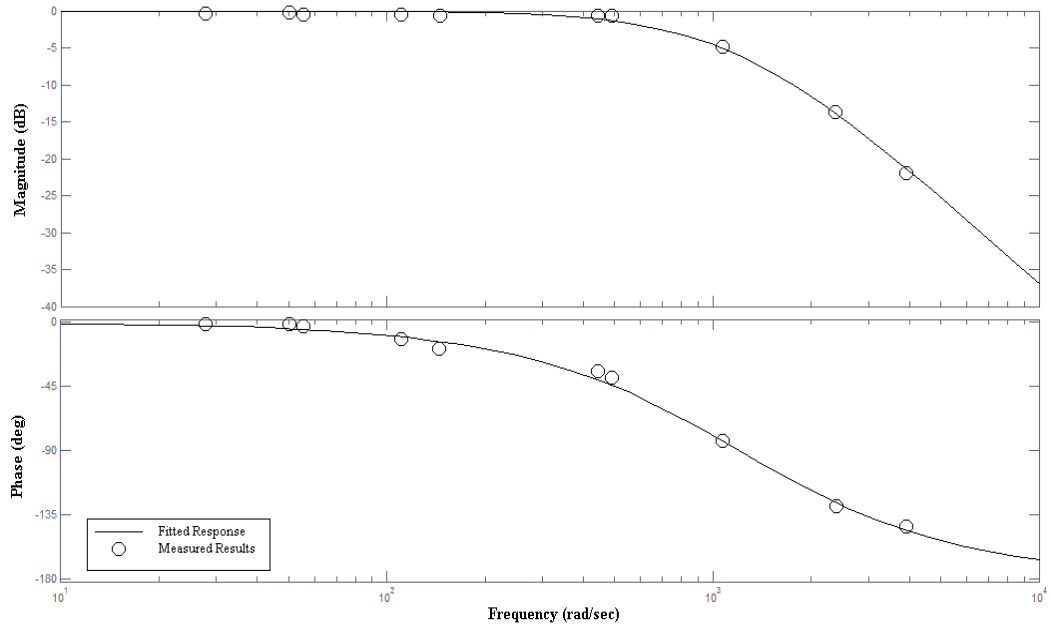

Figure 5.3: Frequency response of SMR [20]

Therefore transfer function of SMR is:

$$G_{SMR} = 36\frac{1200^2}{(s+1200)^2} \tag{5.5}$$

5.2.2 Open-Loop Characteristics of the System

The output current of the switched-mode rectifier is divided into three:

$$I_{OUT}(s) = I_C(s) + I_R(s) + I_B(s) \tag{5.6}$$

Where I_C is the current that flows through the capacitor which charges up to produce the output voltage, I_R is the current flowing through the electrical loads of the vehicle and I_B is the battery current. It has been assumed that the alternator, the battery and the electrical loads are correctly matched to each other, so that sufficient charge of

the battery is maintained. Therefore, in steady-state conditions the battery current flows from the output of the switched-mode rectifier to the battery and does not get reversed to feed the electrical loads.

The charging transfer function of the modeled lead-acid battery was detailly analyzed in Section 2.4.1.1 and Equation (2.11) was derived. It has been shown that the transfer function of the battery is a function of internal resistance, hence SOC. The amplitude of the current drawn through the charging process is a function of VOC which is also dependent on SOC. The change of VOC (Figure 2.18) and the parameters of battery transfer function (Figure 2.17) for specified values of SOC are listed in Table 5.2 and open-loop block diagram of the system is shown in Figure 5.5.

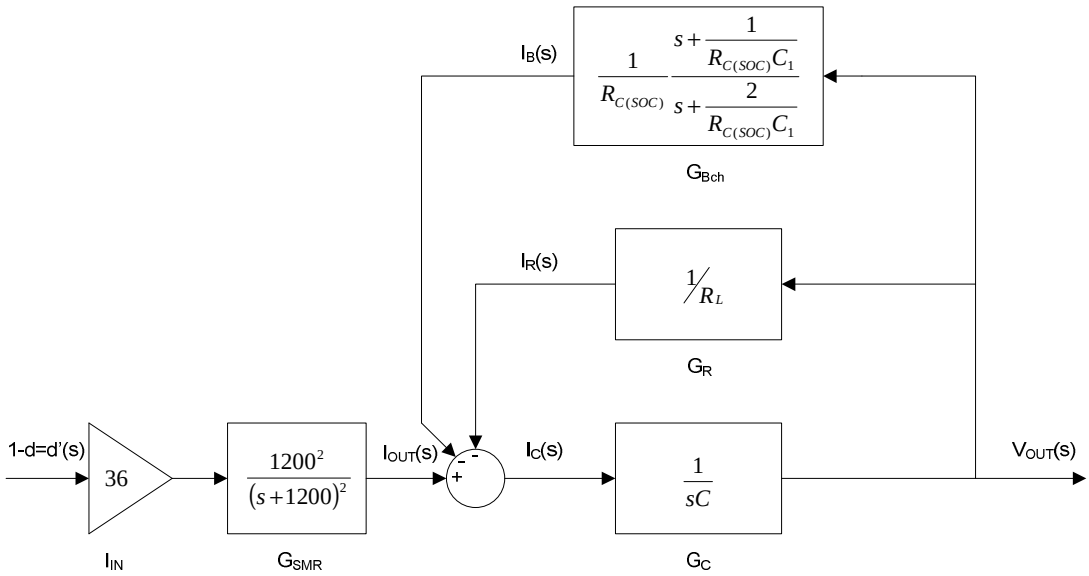

Figure 5.4: Block diagram of open-loop system

For the simplicity of the mathematical analysis and controller design, the effect of VOC in the open-loop block diagram is neglected, because only the amplitude of the battery current is defined by the open circuit voltage, whereas the characteristic by the internal resistance.

By analyzing the input-output relationships in the block-diagram, the open-loop transfer function can be derived:

$$\frac{V_{OUT}}{d'} = \frac{G_{SMR}G_C}{1 + G_C G_R + G_C G_{Bch}} \qquad \textbf{(5.7)}$$

Table 5.1: Open Circuit Voltage and Battery Charging Transfer Function Parameters for Specified Values of State-of-Charge

SOC	VOC	POLE (P_{Bch}) $-2/R_{C(SOC)}C_1$	ZERO (Z_{Bch}) $-1/R_{C(SOC)}C_1$	GAIN (K_{Bch}) $1/R_{C(SOC)}$
10%	11.68	-22.99	-11.49	2.874
20%	11.77	-22.99	-11.49	2.874
30%	11.87	-22.99	-11.49	2.874
40%	11.96	-22.99	-11.49	2.874
50%	12.06	-22.99	-11.49	2.874
60%	12.15	-22.99	-11.49	2.874
70%	12.25	-22.69	-11.35	2.836
80%	12.34	-20.27	-10.13	2.533
90%	12.42	-16.3	-8.149	2.037
100%	12.51	-12.41	-6.203	1.551

The open-loop transfer function of the system can be calculated as follows:

$$\frac{V_{OUT}}{d'} = \frac{36\ 1200^2 R_L\left(s+\frac{2}{R_{C(SOC)}C_1}\right)}{(s+1200)^2\left(\begin{array}{l} s^2 R_L C + s\left(R_L C\frac{2}{R_{C(SOC)}C_1} + R_L\frac{1}{R_C}+1\right) \\ +\left(\frac{2}{R_{C(SOC)}C_1} + R_L\frac{1}{R_{C(SOC)}}\frac{1}{R_{C(SOC)}C_1}\right)\end{array}\right)} \quad \textbf{(5.8)}$$

Note that Equation (5.8) is arranged such that the parameters of battery transfer function can easily be noticed. The value of the capacitor of SMR has a constant value of 3000μF. R_L represents the loads of vehicle electrical system and varies with the consumers, which are activated. Here the value of R_L is considered as a constant value (0.5Ω) representing the maximum current consumption of the electrical loads.

By using the numerical values of the mentioned parameters Equation (5.8) can be rewritten as follows:

$$\frac{V_{OUT}}{d'} = \frac{36\ 1200^2 0.5\left(s + \frac{2}{R_{C(SOC)}C_1}\right)}{(s+1200)^2\left(s^2 0.0015 + s\left(0.0015\frac{2}{R_{C(SOC)}C_1} + 0.5\frac{1}{R_C} + 1\right) + \left(\frac{2}{R_{C(SOC)}C_1} + 0.5\frac{1}{R_{C(SOC)}}\frac{1}{R_{C(SOC)}C_1}\right)\right)} \quad \textbf{(5.9)}$$

In other words:

$$\frac{V_{OUT}}{d'} = \frac{36\ 1200^2 0.5(s - P_{Bch})}{(s+1200)^2\left(s^2 0.0015 + s(-0.0015\ \ P_{Bch} + 0.5K_{Bch} + 1) + (-P_{Bch} - 0.5K_{Bch}Z_{Bch})\right)} \quad \textbf{(5.10)}$$

where P_{Bch}, Z_{Bch} and K_{Bch} are pole, zero and gain value of battery charging transfer function (Table 5.1). Open form of the open-loop transfer function is as follows:

$$\begin{aligned}\frac{V_{OUT}}{d'} = \frac{36\ 1200^2 0.5(s - P_{Bch})}{} \\ s^4 0.0015 + s^3(-0.0015P_{Bch} + 0.5K_{Bch} + 4.6) \\ + s^2(-P_{Bch} - 0.5K_{Bch}Z_{Bch} - 3.6P_{Bch} + 1200K_{Bch} + 4560) \\ + s(-2400P_{Bch} - 1200K_{Bch}Z_{Bch} - 2160P_{Bch} + 720000K_{Bch} + 1440000) \\ -1440000P_{Bch} - 720000K_{Bch}Z_{Bch}\end{aligned} \quad \textbf{(5.11)}$$

Figure 5.6 shows pole-zero map of open-loop transfer function from SOC of 60% to 100%. The change of small poles is shown detailly in Figure 5.7.

5.2.3 Closed-Loop Analysis of the System

The goal of closed-loop system design is to regulate the output voltage of the electrical system powered by a PMSM alternator for various engine speeds, electrical load and SOC conditions. As discussed in Section 5.2.2 open-loop transfer function is dependent on SOC, therefore the closed-loop controller should not be designed without considering it.

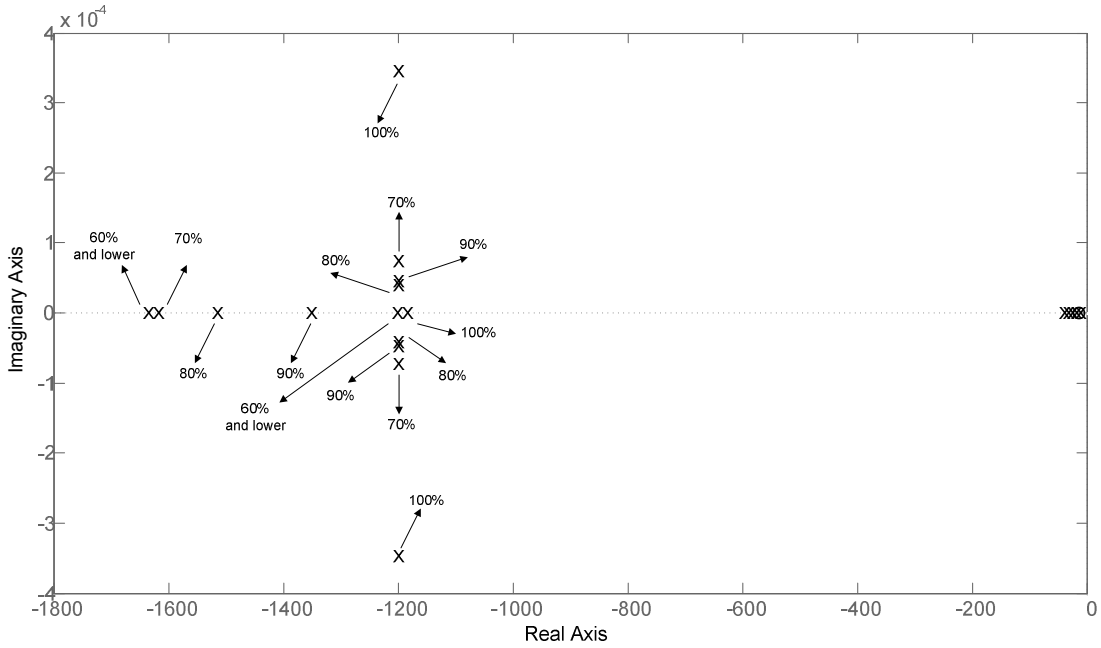

Figure 5.5: Pole-zero map of open-loop transfer function

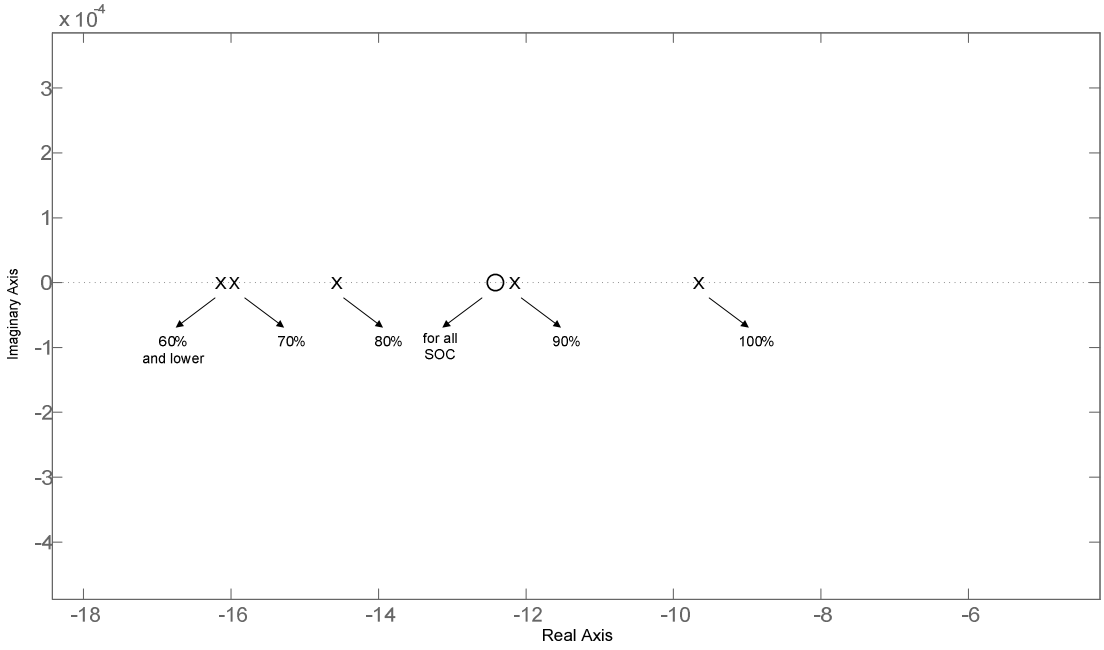

Figure 5.6: Detailed view of pole-zero map for small poles

As shown in Figure 5.6 poles of battery charging transfer function are very close to the coordinate axis and the proximity increases with SOC. It is stated in [21, 22] that, system response was defined by the poles closest to the imaginary axis in the s-plane. Poles farther to the left in the s-plane are associated with natural signals that decay faster than those associated with poles close to the imaginary axis. Therefore, the farther to the left the dominant poles move in the s-plane, the faster the system response becomes.

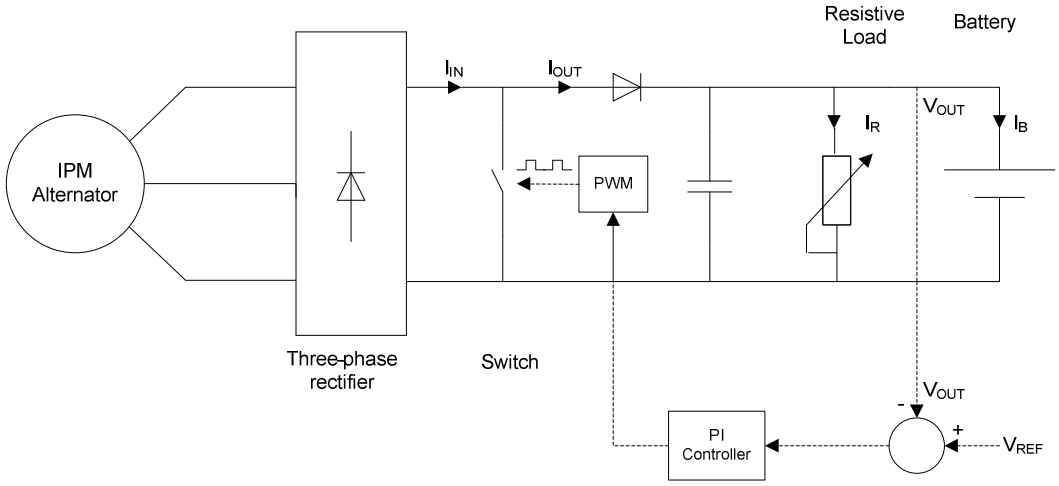

Figure 5.7: Block diagram of closed-loop controlled vehicular electric system

As stated in Equation (5.6) a part of alternator's output current, I_{OUT} is used to charge up the battery. The change of battery charge current versus state-of-charge was given in Figure 2.15. The higher SOC is, the lower gets the charge current, because as shown in Figure 2.18 the higher SOC is the higher gets the VOC and comes closer to the battery terminal voltage.

In Section 5.2.2 it was mentioned that the effect of VOC in the open-loop block diagram was neglected, because only the amplitude of the battery current varies with VOC. Therefore, although the poles of battery charging transfer function gets closer to the coordinate axis with increasing SOC, the battery charging current is higher with decreasing SOC. Thus, controller should be designed for the open-loop transfer function, where battery parameters of lower SOC conditions are used:

$$\frac{V_{OUT}}{d'} = \frac{1.728\ 10^{10}(s+22.99)}{s^4 + 4.0477\ 10^3 s^3 + 5.420\ 10^6 s^2 + 2.4358\ 10^9 s + 3.7922\ 10^{10}} \qquad \textbf{(5.12)}$$

5.2.4 Closed-Loop Design of the System

In order to define the controller type, unity feedback response and steady-state error of the system should be evaluated. Steady-state error is defined as:

$$e_{ss} = \lim_{s\to 0} \frac{sR(s)}{1+G(s)} = \lim_{s\to 0} \frac{R}{1+G(s)} = \frac{R}{1+\lim_{s\to 0} G(s)} \qquad \textbf{(5.13)}$$

G(s) is the open-loop transfer function of the system, which is given in Equation (5.13). Therefore steady-state error is 1.22V for input of 14V. Figure 5.8 shows the unity feedback response of the modeled system for cases where battery is connected and not connected.

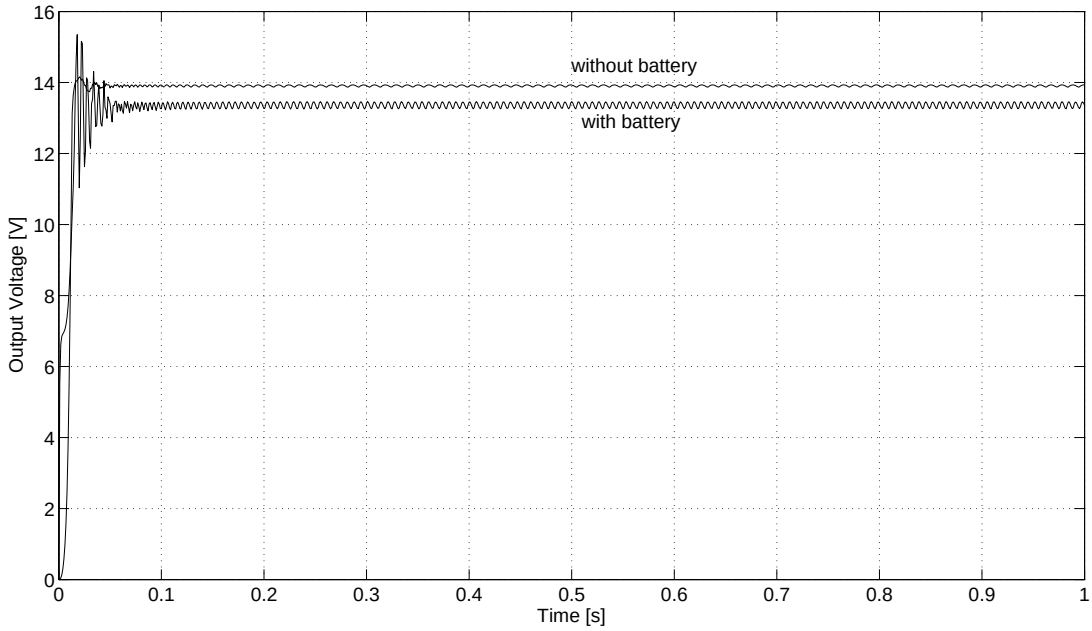

Figure 5.8: Unity feedback responses of electrical system with and without the battery

It is obvious that steady-state error is greater when the battery is connected. In [20] a proportional controller has been proposed for the system without the battery connected. As the steady-state error is greater and nonnegligible for the system with the battery connected, a proportional-integral (PI) controller is required.

$$K_P + \frac{K_I}{s} = \frac{sK_P + K_I}{s} = \frac{K_P\left(s + \frac{K_I}{K_P}\right)}{s} \qquad \textbf{(5.14)}$$

As shown in Equation (5.14) PI controller adds a zero to the open-loop transfer function at $s=-K_I/K_P$ and a pole at $s = 0$. Therefore, the order of the system is increased by one and steady-state error of original system without integral control is improved by an order of one. In other words, if the steady-state error to a given input is constant, the PI controller reduces it to zero [22]. Coefficients of PI controller should be adjusted such that, the zero at $s=-K_I/K_P$ cancels the effect of the small valued pole coming from the battery charging transfer function, which defines the

system response. Referred to Figure 5.9, which shows the closed-loop system response for the open-loop transfer function given in Equation (5.12) for different K_I/K_P ratios, coefficients of PI controller is chosen such that K_I/K_P is 50, because it gives the best result in all SOC values. The output voltage of closed-loop system is shown in Figure 5.10.

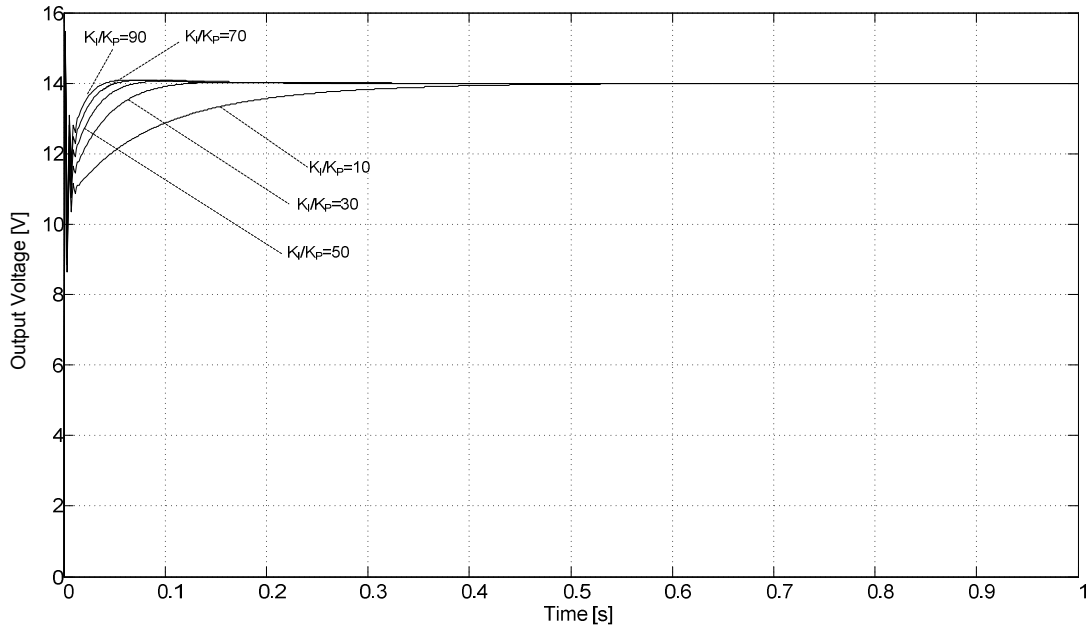

Figure 5.9: Closed-loop system response of PI controller for K_I/K_P ratios

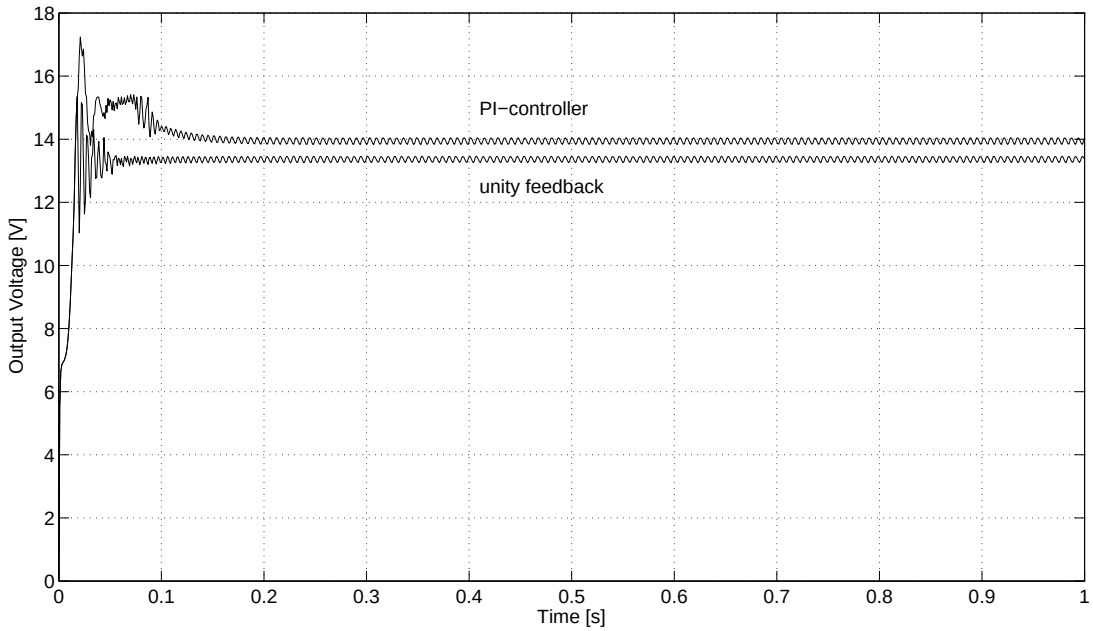

Figure 5.10: Closed-loop response of modeled system

Note that, even though the settling times of the closed-loops response of the modeled system, shown in Figure 5.10 and the one in Figure 5.9 are similar with each other, their transient responses are quite different. This is because; through the mathematical analysis, mean values of the states have been used. When simulation is derived with the complete models of the alternator and the battery, some transient effects may occur. As it is going to be shown in the simulation results on next section, this difference has no important effect on continuous operation of the proposed vehicular electric system.

6. SIMULATION RESULTS

The change of output voltage at variable alternator speed, constant vehicle electrical load and 50% SOC conditions is given in Figure 6.1. Although alternator speed varies between 1200 rpm and 12000 rpm, output voltage is kept constant. The change of complement of duty-cycle (d') at the same operational conditions is given in Figure 6.2. Note that, at high speeds and steady-state conditions, duty-cycle does not vary with speed. As stated in Sections 4.2.2 and 4.2.3, this is because alternator back-EMF is much greater than the output voltage. The input current, as shown in Figure 4.10, is constant and independent of speed. Therefore, as the load conditions are constant, there is no need for the controller to adjust the duty ratio.

It is observed in Figure 6.2, that duty ratio increases at lower alternator speeds, because the alternator back-EMF is smaller than output voltage at this speed range and SMR acts as a boost rectifier.

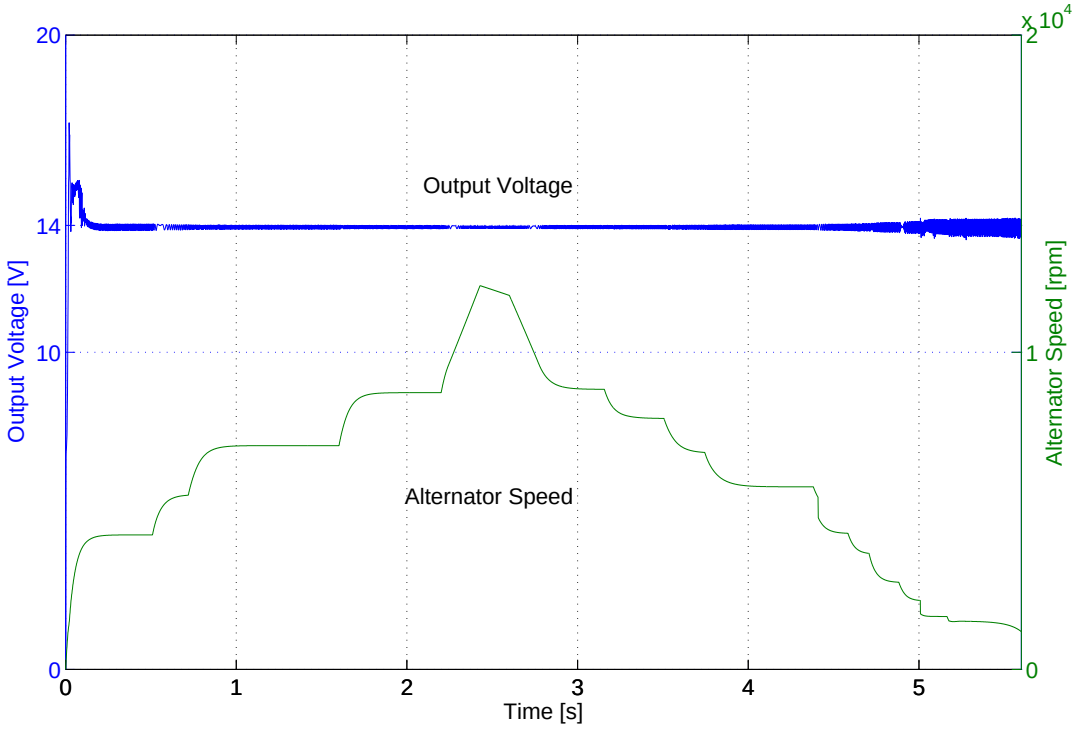

Figure 6.1: Output voltage for variable speed, 50% SOC and constant load conditions

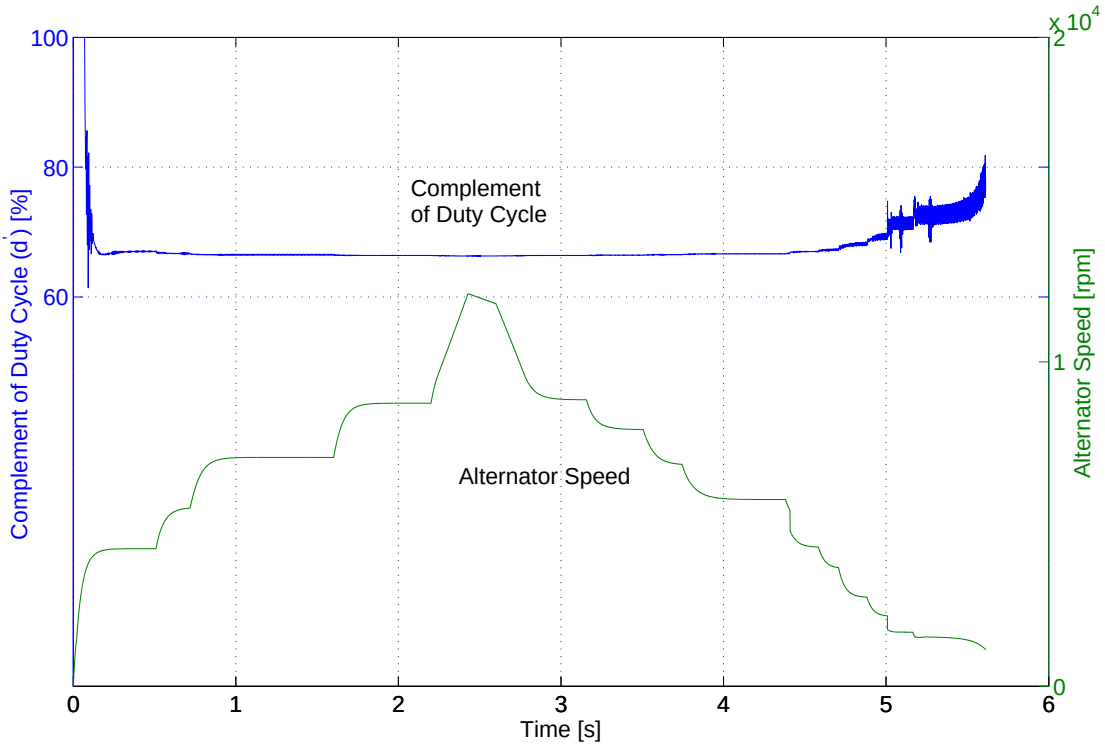

Figure 6.2: Complement of duty cycle (d') for variable speed, 50% SOC and constant load conditions

Figure 6.3 shows the change of output voltage at 50% SOC and variable vehicle electrical load conditions. Figure 6.4 shows the change of complement of duty-cycle (d') at the same operational conditions. As electrical loads on the vehicle change, the current required for the operation of those loads changes accordingly. Therefore, the controller adjusts the duty ratio, hence the output current of SMR to match the output current to the new load condition (Figure 4.9).

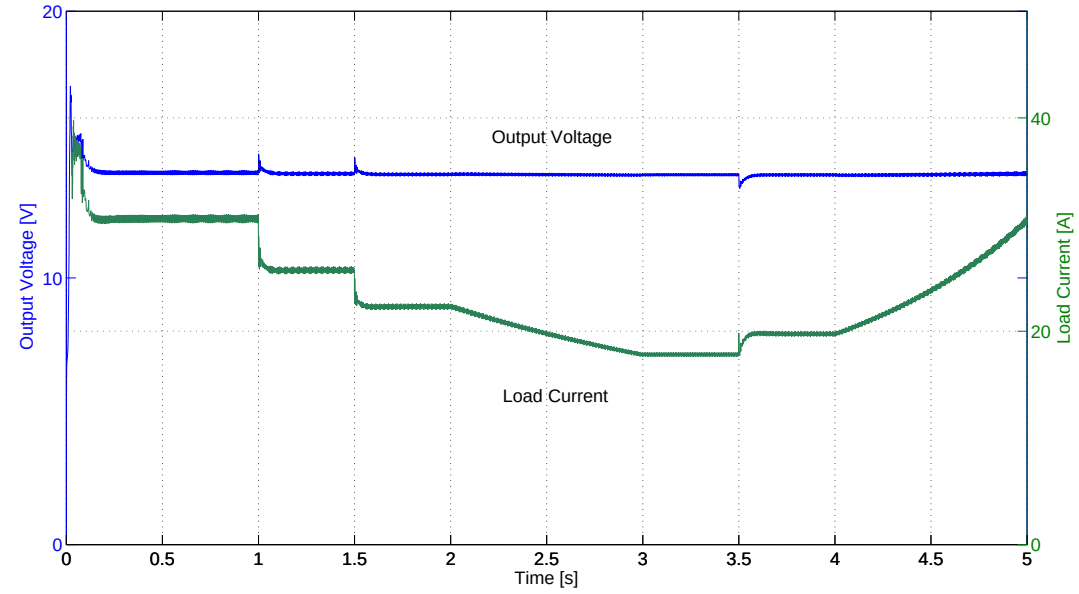

Figure 6.3: Output voltage for variable electrical load conditions at 6000 rpm and 50% SOC

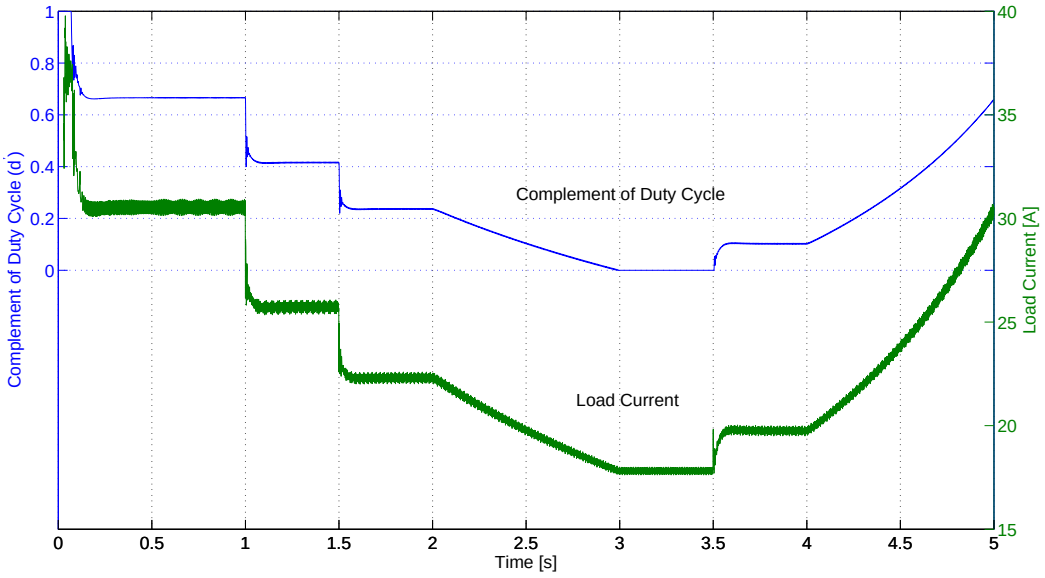

Figure 6.4: Duty-cycle (d') for variable electrical load conditions at 6000 rpm and 50% SOC

As stated in Section 5.2.2 and 5.2.3, the open-loop system and the design of closed-loop system is dependent on SOC conditions of the lead-acid battery. As listed in Table 5.2, over 60% SOC, charging internal resistance, hence transfer function of lead-acid battery differs. Figure 6.5 and Figure 6.6 show the output voltage of closed-loop system at different SOC conditions. Figure 6.5 shows the output voltages at higher SOC. Note that transient responses are different from each other. But in

Figure 6.6, which shows the output voltages at lower SOC, transient responses are not different. These results support the findings given in Table 5.2 and Figure 2.17. It also shows that the designed controller properly operates for all SOC conditions.

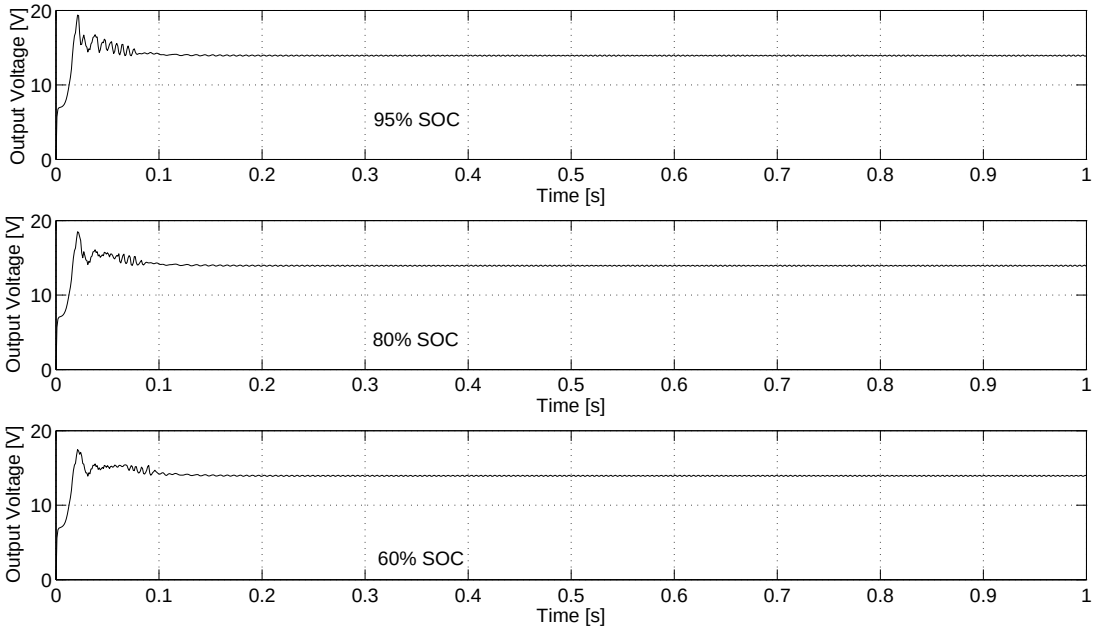

Figure 6.5: Output voltage for higher SOC values at 6000 rpm

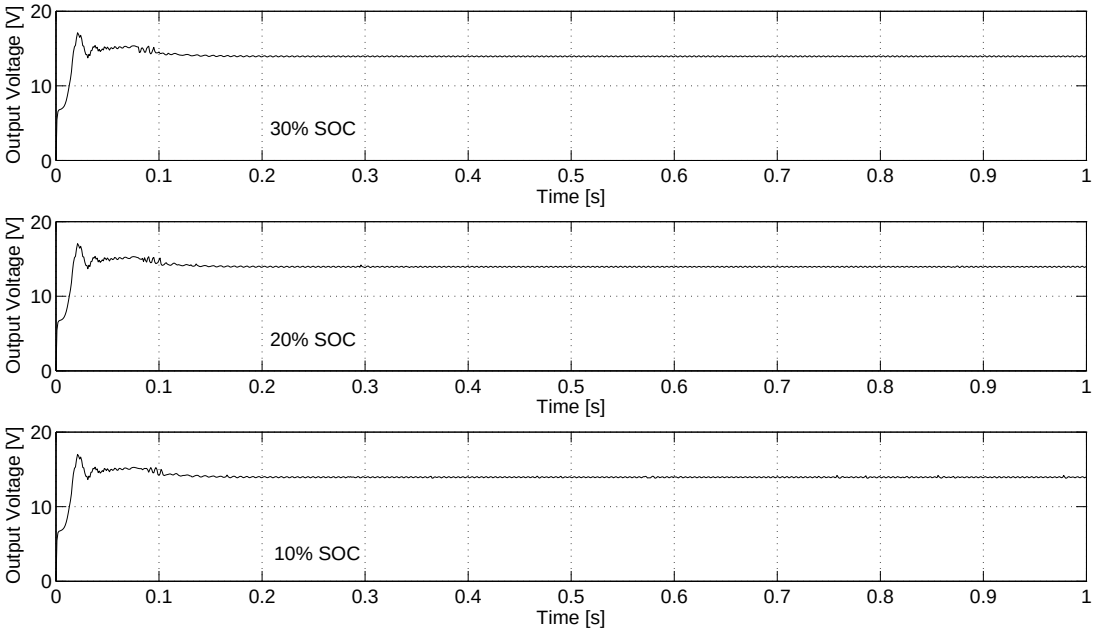

Figure 6.6: Output voltage for lower SOC values at 6000 rpm

7. CONCLUSION

In this study conventional vehicle electrical system has been investigated and a new system has been proposed. The structure and voltage regulation of Lundell-type machine has been introduced, which is still the most common automotive alternator in the market. The properties and performance parameters of lead-acid battery has been discussed and as it is the integral part of vehicle electrical system, a proposed mathematical model of lead-acid battery has been analyzed and simulated in MATLAB/Simulink. By using the equivalent circuit, mathematical analysis has been derived and transfer functions for charge and discharge processes have been calculated. It has been detected that transfer functions for charge and discharge processes are similar, but the transfer function for charging process represents the admittance of the battery, whereas the discharging process the impedance. Therefore, the impedance of the battery is characterized with the discharging resistance and the admittance with the charging resistance.

Because the number of electrical loads in the vehicles is increasing rapidly and Lundell technology is nearing its limits, a high efficiency and high power density electrical system is required. Many different electrical machines have been analyzed and permanent magnet synchronous machine has been proposed and its advantages have been discussed.

For a permanent magnet synchronous machine whose back-EMF voltage is large as compared with the output voltage, the output current will not be significantly affected by speed; hence alternator can be modeled by a constant current source. Therefore, for the output voltage regulation of permanent magnet synchronous machine switched-mode rectifier has been proposed and its operational principles have been discussed.

The open-loop transfer function of the entire system has been derived by combining the transfer function of the switched-mode rectifier and battery. As the parameters of battery transfer function are dependent on state-of-charge, the change of pole-zero locations of open-loop transfer function with the battery state-of-charge has been investigated. It has been detected that, if battery is implemented inside the system, which is composed of permanent magnet synchronous machine, switched-mode

rectifier and vehicle electrical loads, a nonnegligible steady-state error occurs. It has been detected that a pole, which is very close to imaginary axis of s-plane, comes from the battery transfer function. Therefore, a PI controller has been proposed and designed for the closed-loop control of the system.

Closed-loop system has been modeled and simulated for various speed, state-of-charge and electrical load conditions. It has been detected that a successful voltage regulation is maintained even at low speeds in a permanent magnet synchronous machine powered; switched-mode rectifier regulated, lead-acid battery connected and PI regulated vehicle electrical system.

For future works, lead-acid battery model can be changed with lithium-ion battery model. Designed system and battery model can also be used in other power electronics applications, such as hybrid vehicle and wind power plants. In this study, a 14V rated vehicle electrical system has been issued, but in commercial vehicles rated output voltage is 28V and two 12V rated lead-acid batteries are connected in series. Therefore, the battery transfer function and system open-loop characteristics can be investigated for batteries connected in series. Especially in buses, because of the high power air conditioning unit, two alternators operate in parallel. Therefore, parallel operation of switched-mode rectifier regulated permanent magnet synchronous machines can also be investigated.

REFERENCES

[1] **Robert Bosch GmbH,** 2004, Automotive Electrics Automotive Electronics, Bentley Publishers, Cambridge.

[2] **Robert Bosch GmbH,** 2004, Automotive Handbook, SAE Society of Automotive Engineers, Warrendale.

[3] **Lee W., Sunwoo M.,** 2001, Vehicle electric power simulator for optimizing the electric charging system, *International Journal of Automotive technology,* Volume 2, No 4, 157-164.

[4] **Cho P. C., Crecelius D. R.,** 1999, Vehicle alternator/generator trends toward next millennium, *Vehicle Electronics Conference Proceedings of the IEEE International,* Volume 1, 433-438.

[5] **Design and Analysis Software for Electromagnetics,** http://www.infolytica.com/, 19.04.2008.

[6] Linden **D., Reddy T.B.,** 2002, Handbook of Batteries, McGraw-Hill, Newyork.

[7] **Salameh Z. M., Casacca M. A., Lynch W.A.,** 1992, A mathematical model for lead-acid batteries, *IEEE Transactions on Energy Conversion,* Volume 7, No 1, 93-98.

[8] **Ceraolo M.,** 2000, New dynamical model of lead-acid batteries, *IEEE Transactions on Power Systems,* Volume 15, No 4, 1184-1190.

[9] **Dürr M., Cruden A., Gair S., Mcdonald J. R.,** 2005, Dynamical model of a lead-acid battery for use in a domestic fuel cell system, *Journal of Power Sources,* 161, 1400-1411.

[10] **Perrault D. J., Caliskan V.,** 2004, Automotive Power Generation and Control, *IEEE Transactions on Power Electronics,* Volume 19, No 3, 618-630.

[11] **Naidu M., Boules N., Henry R.,** 1997, A high-efficiency high-power-generation system for automobiles, *IEEE Transactions on Industry Applications,* Volume 33, No 6, 1535-1543.

[12] **Martinez-Munoz D., Alakula M.,** 2003, Comparison between a novel claw-pole electrically magnetized synchronous machine without slip-rings and a permanent magnet machine, *Electric Machines and Drive Conference*, Vancouver, Canada, 1-4 June, 1351-1356.

[13] **Krause P. C., Wasynczuk O., Sundhoff S. D.,** 1995, Analysis of Electric Machinery, IEEE Press, Piscataway, New Jersey.

[14] **Jahns T. M., Caliskan V.,** 1999, Uncontrolled generator operation of interior PM synchronous machines following high-speed inverter shutdown, *IEEE Transactions on Industry Applications,* Volume 35, No 6, 1347-1357.

[15] **Bayram T., Stephan A.,** 2006, Comparative study of power electronics converters associated to variable speed permanent magnet alternator, *International Symposium on Power Electronics, Electrical Drives, Automation and Motion SPEEDAM,* Taormina (Sicily), Italy, 23-26 May, 1332-1337.

[16] **Van Niekerk,** 1996, Permanent magnet alternators for standalone electricity generation, *IEEE 4th AFRICON Conference*, Africa, 25-27 September, 451-455.

[17] **Liaw C. Z., Whaley D. M., Soong W. L., Ertugrul N.,** 2004, Investigation of inverterless control of interior permanent magnet alternators, *IEEE Industry Applications Conference*, Westin Hotel, Seattle, Volume 1, 276-283.

[18] **Soong W. L., Ertugrul N.,** 2004, Inverterless high-power interior permanent-magnet automotive alternator, *IEEE Transactions on Industry Applications*, Volume 40, No 4, 1083-1091.

[19] **Mergen A. F., Zorlu S.,** 2006, Elektrik Makineleri III Senkron Makineler, Birsen Yayınevi, İstanbul.

[20] **Liaw C. Z., Soong W. L., Ertugrul N.,** 2005, Closed-loop control and performance of an inverterless interior PM automotive alternator, *International Conference on Power Electronics and Drive Systems PEDS*, Kuala Lumpur, Malaysia, 28 November-01 December, Volume 1, 343-348.

[21] **Franklin G. F., Powell J. D., Emami-Naeini A.,** 2006, Feedback Control of Dynamic Systems, Pearson Prentice Hall, New Jersey.

[22] **Kuo B. C., Golnaraghi F.,** 2003, Automatic Control Systems, John Wiley & Sons, New York

RESUME

Berker Bilgin was born in Sakarya in 02 March 1982. He graduated the primary and Anatolian high school in Sakarya. In 2004 he graduated from the electrical engineering program in Istanbul Technical University and began working in Mercedes-Benz Turk A.Ş. (A company of Daimler A.G.) as a service engineer in After-sales department. Since 2008 he works as a testing and prototyping engineer in Bus Development department in Mercedes-Benz Turk A.Ş.